Impact of mineral dust on the global nitrate aerosol direct and indirect radiative effect

Alexandros Milousis[1], Klaus Klingmüller[2], Alexandra P. Tsimpidi[1], Jasper F. Kok[3], Maria Kanakidou[4,5,6], Athanasios Nenes[5,7], and Vlassis A. Karydis[1]

[1]Institute of Energy and Climate Research, Forschungszentrum Jülich GmbH, Jülich, Germany
[2]Max Planck Institute for Chemistry, Mainz, Germany
[3]Department of Atmospheric and Oceanic Sciences, University of California — Los Angeles, Los Angeles, CA, USA.
[4]Environmental Chemical Processes Laboratory, Department of Chemistry, University of Crete, Heraklion, Greece
[5]Center for the Study of Air Quality and Climate Change, Foundation for Research & Technology Hellas, Patras, Greece
[6]Institute of Environmental Physics, University of Bremen, Bremen, Germany
[7]Laboratory of Atmospheric Processes and Their Impacts, Ecole Polytechnique Fédérale de Lausanne, Switzerland

Abstract

Nitrate (NO_3^-) aerosol is projected to increase dramatically in the coming decades and may become the dominant inorganic particle species. This is due to the continued strong decrease in SO_2 emissions, which is not accompanied by a corresponding decrease in NO_x and especially NH_3 emissions. Thus, the radiative effect (RE) of NO_3^- aerosol may become more important than that of SO_4^{2-} aerosol in the future. The physicochemical interactions of mineral dust particles with gas and aerosol tracers play an important role in influencing the overall RE of dust and non-dust aerosols but can be a major source of uncertainty due to their lack of representation in many global climate models. Therefore, this study investigates how and to what extent dust affects the current global NO_3^- aerosol radiative effect through both radiation (RE_{ari}) and cloud interactions (RE_{aci}) at the top of the atmosphere (TOA). For this purpose, multi-year nudged simulations towards the observed atmospheric circulation were performed with the global atmospheric chemistry and climate model EMAC, while the thermodynamics of inorganic aerosols and dust interactions were simulated with the thermodynamic equilibrium model ISORROPIA-lite. The emission flux of the mineral cations Na^+, Ca^{2+}, K^+ and Mg^{2+} is calculated as a fraction of the total aeolian dust emission based on the unique chemical composition of the major deserts worldwide. Our results reveal positive and negative shortwave and longwave radiative effects in different regions of the world via aerosol-radiation interactions and cloud adjustments. Overall, the NO_3^- aerosol direct effect contributes to a global cooling of -0.11 W/m^2, driven by coarse-mode particle cooling at short wavelengths. The simulated global average direct effect of NO_3^- aerosol is reduced to -0.09 W/m^2 when mineral dust is assumed to be chemically inert, but also when it is assumed to have a homogeneous chemical composition with respect to mineral ions. If mineral dust emissions are reduced by half, the average direct effect of NO_3^- aerosol is reduced to -0.08 W/m^2, while a 50% increase in the global dust load leads to a cooling of -0.10 W/m^2. Regarding the indirect effect, it is noteworthy that NO_3^- aerosol exerts a global mean warming of +0.17 W/m^2. While the presence of NO_3^- aerosol enhances the ability of mineral dust particles to act as cloud condensation nuclei (CCN), it simultaneously inhibits the formation of cloud droplets from the smaller anthropogenic particles. This is due to the coagulation of fine anthropogenic CCN particles with the larger mineral dust particles, which limits the total aerosol number concentration. This mechanism results in an overall reduced cloud albedo effect and is thus attributed as warming. Sensitivity simulations showed that the calculated warming is sensitive to both mineral dust load (+0.14 W/m^2) and composition (+0.11 W/m^2).

Keywords: radiative forcing, direct radiative effect, indirect radiative effect , nitrate aerosols, mineral dust,

1. Introduction

Atmospheric aerosols are among the most complex components of the Earth's climate system. This is due not only to the diversity of their origins, with many natural and anthropogenic emission sources, but also to their extremely varied chemical composition and properties. The many mechanisms by which they interact with each other and with physical entities such as radiation, clouds, land, and oceans add to their complexity and play a critical role in the energy balance of the planet (Arias et al., 2021). The most direct way in which aerosols affect the Earth's energy balance is through their interactions with solar shortwave (SW) and terrestrial longwave (LW) radiation (IPCC, 2013). Overall, the radiative effect due to aerosol-radiation interactions (REari) is mainly dominated by the scattering of SW radiation back to space (negative radiative effect, generating a cooling of the climate system) and the absorption of LW radiation (positive radiative effect, generating a warming of the climate system) (Gao et al., 2018; Tsigaridis and Kanakidou, 2018). Aerosols belonging to the black and/or brown carbon family, together with mineral dust particles, contribute to absorption (Kanakidou et al., 2005; Wong et al., 2019; Zhang et al., 2017), while the main inorganic aerosol components, such as sulfate and nitrate, as well as a significant amount of organic carbon contribute mainly to scattering (Bond and Bergstrom, 2006; Kirchstetter et al., 2004; Klingmüller et al., 2019; Zhang, 2020). However, mineral dust can also influence the behavior of the REari of anthropogenic pollution. Dust particles alter the anthropogenic radiative effect of aerosol-radiation interactions by reducing the loading of anthropogenic aerosols (either by coagulating with them or by adsorption of their precursor inorganic trace gases), leading to less scattering of solar radiation and thus a warming effect (Kok et al., 2023).

Atmospheric aerosols can also indirectly affect the Earth's energy balance by forming clouds, controlling cloud optical thickness and scattering properties, and altering their precipitation and lifetime (IPCC, 2013). Atmospheric aerosols act as cloud condensation nuclei (CCN), providing a suitable surface for water vapor to condense, leading to the formation of liquid droplets that develop into a corresponding liquid cloud (Lance et al., 2004). Such clouds are referred to as warm clouds and are typically found in the lower troposphere (Khain and Pinsky, 2018). However, there is a constant competition between small and large particles for the available amount of water vapor(Barahona et al., 2010; Morales and Nenes, 2014). Under the same humidity conditions, the presence of small particles will lead to the formation of small droplets with high number concentrations, while the presence of larger particles will lead to the formation of large droplets but with lower number concentrations. Depending on the size characteristics of its particle population, a warm cloud will exhibit different optical properties, with a population dominated by smaller particles generally being more reactive in the SW spectrum. The change in cloud reflectivity due to the presence of aerosols is referred to as the first radiative effect due to aerosol-cloud interactions (REaci) and was first described by Twomey (1977). The small size of anthropogenic aerosols results in an overall smaller cloud droplet size, which reduces precipitation efficiency and thus increases cloud lifetime. This contributes to cloud reflectivity and is referred to as the second radiative effect of aerosol cloud-interactions, first described by Albrecht (1989). These two indirect effects are considered equally important for the total indirect radiative effect of aerosols (Lohmann and Feichter, 2005). Atmospheric aerosols exert a net cooling effect that can partially mask the warming effect of greenhouse gases, therefore, the recent decline in anthropogenic aerosol concentrations may accelerate global warming (Urdiales-Flores et al.,

2023). Overall, the radiative effect due to aerosol-cloud interactions is considered the main source of existing uncertainty in the effective (total) radiative effect of aerosols in the atmosphere (Myhre et al., 2014; Seinfeld et al., 2016).

Mineral dust influences the anthropogenic radiative effect through aerosol-cloud interactions in several ways that can result in either a net warming or net cooling effect. Dust particles can increase the number of CDNC in remote areas since through chemical aging by pollutants (Nenes et al., 2014; Karydis et al., 2017), dust particles become more hygroscopic and require lower supersaturation thresholds for activation (Karydis et al., 2011). This is caused by the transfer of anthropogenic pollutants towards remote desert regions which enhances the solubility of dust particles. In such regions, this mostly results in increased cloud albedo and a net cooling effect. However, dust particles also tend to reduce the availability of smaller anthropogenic CCN, mostly through coagulation with them. This is due to intrusions of aged dust particles into polluted environments which reduce the numbers of smaller aerosols through increased coagulation with them. This results in lower cloud reflectivity (albedo) and thus a net warming effect (Klingmüller et al., 2020). Furthermore, when dust is above or below low-level clouds, the resulting effect of local heating is an increase in total cloud cover due to enhanced temperature inversion or enhanced upward vertical motion, respectively (Kok et al., 2023). On the other hand, when dust is present inside low-level clouds, local heating enhances in-cloud evaporation, resulting in an overall decrease in cloud cover. Kok et al. (2023) showed that the amount of desert dust in the atmosphere has increased since the mid-19th century, causing an overall cooling effect on the Earth that masks up to 8% of the warming caused by greenhouse gases. If the increase in dust were halted, the previously hidden additional warming potential of greenhouse gases could lead to slightly faster climate warming.

NO_3^- is expected to dominate the global aerosol composition in the coming decades due to the predicted limited availability of SO_4^{-2} following the abrupt decline in SO_2 emissions, which will not necessarily be accompanied by proportional reductions in NO_x and NH_3 emissions (Bellouin et al., 2011; Hauglustaine et al., 2014). Excess NO_3^- is expected to exert a cooling RE_{ari} by scattering SW radiation (Bauer et al., 2007a; Xu and Penner, 2012; Myhre et al., 2013; IPCC, 2013; Li et al., 2015), but the RE_{aci} is much more complex and complicated and can lead to both cooling and warming. Mineral dust thus becomes a key factor, as it is one of the main promoters of NO_3^- aerosol formation, providing a very suitable surface for gaseous HNO_3 condensation to the aerosol phase (Karydis et al., 2011; Trump et al., 2015). This affects not only the optical properties of dust aerosols (see Fig. 1a), which will influence their overall RE_{ari}, but also how they can alter cloud formation and microphysics (see Fig. 1d). NO_3^- aerosols increase the hygroscopicity of mineral dust (Kelly et al., 2007) by providing layers of soluble material on their surface, thus increasing their ability to act as CCN (Karydis et al., 2017). However, NO_3^- aerosols can also affect dust particles by increasing their size and thus coagulation, resulting in larger particles but lower aerosol number concentrations (Klingmüller et al., 2020). Thus, nitrate-dust interactions are a complex mechanism that ultimately affects climatology in a variety of ways. The role of mineral dust in modifying the influence of NO_3^- aerosols in the global RE_{aci} is not yet well understood. This study aims to focus on the extent of the RE_{ari} and RE_{aci} of NO_3^- aerosols and on how interactions with mineral dust regulate both on a global scale.

This study is organized as follows: in Section 2, details of the modeling setup for conducting the global simulations as well as the treatment of dust-nitrate interactions in the model are discussed and the methodology for calculating the global RE_{ari} and RE_{aci} of NO_3^- aerosols is explained. Section 3 presents the main results for the global RE_{ari} for coarse and fine NO_3^- aerosols for the base case simulation and the sensitivity cases listed in Table 1. Section 4 presents the results for the global RE_{aci} of total NO_3^- aerosols, while section 5 includes the feedback mechanism of dust-nitrate interactions with cloud microphysics. Finally, the main conclusions and a general discussion on the scope of the study are presented in section 6.

2. Methodology

2.1 Model Setup

The simulations were performed with the global atmospheric chemistry and climate model EMAC (ECHAM/MESSy) (Jockel et al., 2006), which includes several submodels describing atmospheric processes and their interactions with oceans, land, and human influences. These submodels are linked through the Modular Earth Submodel System (MESSy) (Jockel et al., 2005) to a base model, the 5th Generation European Center Hamburg General Circulation Model (ECHAM) (Roeckner et al., 2006). The submodel system used in this work includes the MECCA submodel, which performs the gas phase chemistry calculations (Sander et al., 2019). The SCAV submodel is responsible for the in-cloud liquid-phase chemistry and wet deposition processes (Tost et al., 2007b; Tost et al., 2006), while DRYDEP and SEDI are used to compute the dry deposition of gases and aerosols and gravitational settling, respectively (Kerkweg et al., 2006). All aerosol microphysical processes are calculated by the GMXe submodel (Pringle et al., 2010a; Pringle et al., 2010b), where aerosols are divided into 4 lognormal size modes (nucleation, Aitken, accumulation and coarse). The mean radius for each mode is 1.7 nm, 19 nm, 205 nm and 2213 nm respectively with a sigma equal to 1.59 for the first three and 2 for coarse mode. The partitioning between the gas and aerosol phases is calculated using the ISORROPIA-lite thermodynamic module (Kakavas et al., 2022) as implemented in EMAC by Milousis et al. (2024). The optical properties of the aerosols and the radiative transfer calculations are simulated by the submodels AEROPT (Dietmuller et al., 2016) and RAD (Dietmuller et al., 2016), respectively. AEROPT can be called several times within a model time step with different settings for the aerosol properties. More details are given in section 2.3.1. All cloud properties and microphysical processes are simulated by the CLOUD submodel (Roeckner et al., 2006) using the two-moment microphysical scheme of Lohmann and Ferrachat (2010) for liquid and ice clouds. The activation processes of liquid cloud droplets and ice crystals follow the physical treatment of Morales and Nenes (2014) and Barahona and Nenes (2009), respectively, as described by Karydis et al. (2017) and Bacer et al. (2018). More details are given in Section 2.3.2.

The meteorology for each of the simulations was nudged by ERA5 reanalysis data (C3S, 2017), thus this study estimates the radiative effect of nitrate aerosols with respect to REari and REaci separately, rather than the total effective radiative effect, as this would require multiple free-run simulations with prescribed sea surface temperatures for each case separately. The spectral resolution used for each simulation was T63L31, which corresponds to a grid resolution of 1.875^o x 1.875^o and 31 vertical layers up to 25 km in height. The period covered by the simulations is from 2007 to 2018, with the first year representing the model spin-up period.

Anthropogenic aerosol and trace gas emissions were taken from the CMIP6 database (O'Neill et al., 2016) according to the SSP370 scenario. Natural NH_3 emissions (from land and ocean) were based on the GEIA database (Bouwman et al., 1997), and natural volcanic SO_2 emissions were taken from the AEROCOM database (Dentener et al., 2006). Biogenic NO emissions from soils were calculated online according to the algorithm of Yienger and Levy (1995), while lightning-produced NO_x was also calculated online by the LNOx submodel (Tost et al., 2007a) using the parameterization of Grewe et al. (2001). DMS emissions from the oceans are calculated online by the AIRSEA submodel (Pozzer et al., 2006). Sea salt emissions are based on the AEROCOM database (Dentener et al., 2006) following the chemical composition reported by Seinfeld and Pandis (2016), i.e. 30.6% Na^+, 3.7% Mg^+, 1.2% Ca^{2+}, 1.1% K^+, and 55% Cl^-. Dust emissions are calculated online using the parameterization of Astitha et al. (2012), which considers the meteorological information for each grid cell (i.e., temperature and relative humidity), as well as the different thresholds of frictional velocities above which dust particle suspension occurs. Dust particles are emitted in the accumulation and coarse size modes of the insoluble fraction, but can be transferred to the soluble fraction after either coagulation with other soluble species and/or by condensation of soluble material on their surface. Both processes are treated and calculated by GMXe and ISORROPIA-lite. The emissions of mineral ions (Ca^{2+}, Mg^{2+}, K^+, and Na^+) are estimated as a fraction of the total dust emission flux based on the soil chemical composition of each grid cell. This is done using desert soil composition maps from Klingmüller et al. (2018) which are based on the mineral ion fractions from Karydis et al. (2016). To assess the impact of changes in mineral dust chemistry and emissions on the global NO_3^- aerosol RE_{ari} and RE_{aci}, four additional sensitivity simulations were performed (Table 1). In the first sensitivity simulation, mineral dust is described only by a bulk, chemically inert species. In the second sensitivity case, the chemical composition of the mineral dust was assumed to be spatially uniform, with a percentage distribution for bulk dust, Na^+, K^+, Ca^{2+} and Mg^{2+} particles assumed to be 94%, 1.2%, 1.5%, 2.4% and 0.9% respectively according to Sposito (1989). Finally, two additional simulations were performed to assess the impact of the global mineral dust budget on the results, where the dust emission fluxes were first halved and then increased by 50% to account for the historical increase in global dust mass load since pre-industrial times, as reconstructed by Kok et al. (2023).

2.2 Treatment of Dust-Nitrate Interactions

The interactions between mineral dust and nitrate aerosols play a crucial role in altering the optical properties of both species, but can also strongly influence cloud microphysical processes (Fig. 1). Therefore, they are of paramount importance in the way that the presence of dust aerosols affects both the RE_{ari} and the RE_{aci} of nitrate aerosols. First, the adsorption of HNO_3 on the surface of dust particles is a process that strongly promotes the formation of nitrate aerosols on dust (Karydis et al., 2016). In this case, the condensation of gaseous species is treated by the GMXe submodel. Specifically, the amount of gas phase species that can kinetically condense within a model time step (equal to 10 minutes in this study) is calculated according to the diffusion limited condensation theory of Vignati et al. (2004). This information is then passed to the ISORROPIA-lite thermodynamic module to calculate the gas/aerosol partitioning. Specifically, the module receives as input the ambient temperature and humidity along with the diffusion limited concentrations of H_2SO_4, NH_3, HNO_3, and HCl, the concentrations of the non-volatile cations

(NVCs) Na^+, K^+, Ca^{2+} and Mg^{2+}, and the concentrations of the ions SO_4^{2-}, NO_3^-, NH_4^+, and Cl^- present in the aerosol phase from the previous time step. It calculates the equilibrium reactions of the NO_3^- anion with the NVCs, among others, depending on their abundance with respect to the SO_4^{2-} anion. Therefore, in all cases where mineral dust is considered chemically active, all reactions of nitrate aerosols with NVC are treated. The coating of dust particles by nitrate aerosols during gas/aerosol partitioning calculations is an important process that leads to an increase in dust solubility and hygroscopicity (Laskin et al., 2005). . Therefore, after these processes have taken place, a large fraction of the originally insoluble dust particles have become soluble (Fig. 1a), a fact that leads to changes in their optical profiles, as their increased ability to absorb water makes them more efficient in extinguishing SW radiation and emissivity of LW radiation (Fig. 1a, 1b) (Kok et al., 2023). The transfer to the soluble fraction after coating with soluble material is handled by the GMXe submodel, which also provides some key aerosol attributes necessary for the calculation of their optical properties (see Section 2.3). In general, the changes in the properties of dust particles through their interactions with nitrate aerosols will result in more efficient removal rates, mainly through wet deposition, due to their higher hygroscopicity and increased size (Fan et al., 2004). The reduced number of dust particles that can act as ice nuclei (IN) and their increased size can lead to an optical thinning of cirrus clouds (Fig. 1c) (Kok et al., 2023). Furthermore, the changes induced by dust-nitrate interactions alter the formation of warm clouds in a way that is particularly detrimental to the smaller aerosols (Fig. 1d). In particular, the enhanced hygroscopicity of dust particles will lead to a faster depletion of the available supersaturation, as they act as giant CCN that absorb large amounts of water vapor to activate into cloud droplets (Karydis et al., 2017). In addition, the population of smaller aerosols will also be depleted by increased coagulation with the large dust particles (Klingmüller et al., 2020). The coagulation of aerosols is also handled by the GMXe submodel, following Vignati et al. (2004) and the coagulation coefficients for Brownian motion are calculated according to Fuchs and Davies (1964). As a consequence of the different degrees of complexity of the dust-nitrate interactions, it is very important to note that they do not always result in a linear response in terms of how they affect climate through their subsequent interactions with radiation, clouds, or both.

2.3 Radiative Effect Calculation

To calculate the global RE_{ari} and RE_{aci} of NO_3^- aerosols, the optical properties from the AEROPT submodel and the radiative transfer calculations from the RAD submodel were used. First, AEROPT provides the aerosol extinction (absorption and scattering) coefficients, the single scattering albedo, and the aerosol asymmetry factor for each grid cell with a vertical distribution analogous to the vertical resolution used. The GMXe submodel is used to provide input of aerosol attributes for the calculation of aerosol optical properties, which is done online using 3D look-up tables. The tables provide information on the real and imaginary parts of the refractive index and the Mie size parameter per size mode (Dietmuller et al., 2016). Then, the radiative scheme of RAD uses the particle number weighted average of the extinction cross section, the single scattering albedo, and the asymmetry factor as input for the radiative transfer calculations. In addition to AEROPT, RAD takes input from the submodels ORBIT (Earth orbital parameters), CLOUDOPT (cloud optical properties) (Dietmuller et al., 2016), and IMPORT (import of external datasets) to

calculate the radiative transfer properties for longwave and shortwave radiation fluxes separately. Both the AEROPT and RAD submodels can be invoked multiple times within a model time step, each time with different settings for the aerosol optical properties, allowing radiative transfer estimates for identical climatological conditions. This is of paramount importance for the calculation of the REari of aerosols since any effects due to possibly different climatological conditions must be eliminated. Henceforth, all references to RE estimates, as well as net, longwave, and shortwave flux quantities, will refer to the top of the atmosphere (TOA) only.

2.3.1 Radiative Effect from Aerosol-Radiation Interactions (RE_{ari})

To estimate the global RE_{ari} of all aerosols as well as that of total, coarse, and fine NO_3^- aerosols, 3 simulations were performed for each sensitivity case in Table 1. In the first simulation all aerosol species are present, in the second simulation NO_3^- aerosols are completely removed by turning off their formation, and in the third simulation coarse mode NO_3^- aerosols are removed by forcing HNO_3 to condense only on the fine mode (i.e., sum of the three smaller lognormal size modes: nucleation, Aitken, and accumulation). For each of these three simulations, the radiative transfer routines are called twice for each time step. One call uses the normal aerosol optical properties, and the other call uses an aerosol optical depth equal to 0 to emulate an atmosphere without aerosols. Essentially, the global RE_{ari} of each simulation can be calculated by taking the difference between the net fluxes between the two calls. More specifically, the first simulation will yield the RE_{ari} of the total aerosol load ($F_{1,ari}$ hereafter), the second simulation will yield the RE_{ari} of all aerosols except NO_3^- ($F_{2,ari}$ below), and the third simulation will yield the RE_{ari} of all aerosols except the coarse mode NO_3^- ($F_{3,ari}$ below). Since the above estimates of the radiative effect were computed using the exact same climatology, its effect was effectively eliminated. However, in order to isolate the NO_3^- aerosol radiative effect, it is also essential to disable any aerosol-cloud interactions, otherwise the cooling effect would be severely underestimated because cloud scattering would make aerosol scattering less relevant (Ghan et al., 2012). For this purpose, the simplest cloud scheme available in the EMAC model is used, which calculates cloud microphysics according to Lohmann and Roeckner (1996) and cloud coverage according to Tompkins (2002). To disable aerosol-cloud interactions, no aerosol activation routines are used to avoid coupling with the activation schemes. Overall, the global RE_{ari} of total, coarse, and fine NO_3^- aerosols are obtained as follows:

- $F_{NO3,ari}(F_{N,ari}) = F_{1,ari} - F_{2,ari}$
- $F_{coarseNO3,ari}(F_{cN,ari}) = F_{1,ari} - F_{3,ari}$
- $F_{fineNO3,ari}(F_{fN,ari}) = F_{3,ari} - F_{2,ari}$

2.3.2 Radiative Effect from Aerosol-Cloud Interactions (RE_{aci})

In this work we estimate the effect of total NO_3^- aerosols on the calculated global RE_{aci}. Climatology plays a crucial role in aerosol-cloud interactions and simulating a "fine-only NO_3^- atmosphere", as done for the RE_{ari} calculations, would produce an unrealistic climatological scenario, since coarse-mode NO_3^- is strongly associated with cations in mineral dust particles

(Karydis et al., 2016), making them quite effective as CCN (Karydis et al., 2017). Therefore, the RE_{aci} calculations require only 2 simulations for each sensitivity case separately: one with all aerosols present and one with the entire NO_3^- aerosol load removed by turning off their formation. The global RE_{aci} is then given by:

- $F_{NO3,aci}(F_{N,aci}) = FF_N - F_{N,ari}$

where FF_N is the total NO_3^- aerosol feedback radiative effect. Since $F_{N,ari}$ is calculated using the methodology described in Section 2.3.1, it is only necessary to estimate FF_N. This is equal to the difference in net fluxes between the two simulations. There is no need to emulate an aerosol-free atmosphere here since any differences induced by different climatologies must be included. The two simulations performed for the calculation of RE_{aci} use the cloud formation scheme as described in Lohmann and Ferrachat (2010), which uses prognostic equations for the water phases and the bulk cloud microphysics. In addition, the empirical cloud cover scheme of Sundqvist et al. (1989) is used. For aerosol activation, the CDNC activation scheme of Morales and Nenes (2014) is used, which includes the adsorption activation of mineral dust as described in Karydis et al. (2017). The effect of dust-nitrate interactions on clouds presented here refers to the lowest level of cloud formation at 940 hPa. For the ICNC activation, the scheme of Barahona and Nenes (2009) is used, which calculates the ice crystal size distribution through heterogeneous and homogeneous freezing as well as ice crystal growth.

3. Radiative Effect from Aerosol-Radiation Interactions (RE_{ari})

3.1 Base Case

The global average RE_{ari} of total NO_3^- aerosols at the top of the atmosphere was found to be -0.11 W/m^2, which is within the reported range of the estimated present day all-sky direct radiative effect of total NO_3^- aerosols by other studies (Bauer et al., 2007a; Bauer et al., 2007b; Liao et al., 2004; Myhre et al., 2013; IPCC, 2013; Xu and Penner, 2012). The NO_3^- cooling of the RE_{ari} calculated by EMAC is driven by the scattering of SW radiation (equal to -0.34 W/m^2), which outweighs the warming due to absorption of LW radiation (equal to +0.23 W/m^2) (Table 2). The RE_{ari} of the total NO_3^- aerosol is dominated by the coarse particles, as they account for 82% of the calculated SW cooling and all of the LW warming (Table 2; Figure 2). The warming effect of the coarse particles is strongest over the dust belt zone and especially over the regions of the Middle East and the northern face of the Himalayan plateau. These regions are characterized by high concentrations of coarse NO_3^- aerosols due to the adsorption of HNO_3 on desert soil particles (Karydis et al., 2016; Milousis et al., 2024). Therefore, the warming due to absorption of terrestrial LW radiation by coarse-mode nitrates interacting with mineral dust is the strongest over these areas (Fig. 1a), reaching up to +4 W/m^2 (Fig. 2iii). On the other hand, the scattering of solar SW radiation is higher over regions with higher concentrations of total NO_3^- aerosols. Over the USA and Europe, the SW RE_{ari} is -1.5 W/m^2 (Fig. 2v). However, the cooling exerted by nitrate aerosol through the SW RE_{ari} is more profound over areas where it interacts strongly with high concentrations of mineral dust particles (Fig. 1b). Such areas include the Congo Basin, where HNO_3 from tropical forest biomass burning interacts with Saharan mineral dust particles; the North

Indian region, where anthropogenic HNO_3 emissions interact with mineral dust particles from the Taklimakan desert; and the East Asian region, where HNO_3 emissions from Chinese megacities interact with mineral dust particles from the Gobi desert. These regions can result in an average cooling of up to -4 W/m^2 (Fig. 2v). Interestingly, cooling through SW interactions is not evident over the Sahara desert, most likely due to the minimal presence of nitrate aerosols in the $PM_{2.5}$ size range (not shown). The high concentrations of nitrate aerosols in the $PM_{2.5-10}$ range over the Sahara contribute to the LW absorption, but the SW scattering is almost exclusively associated with the regions dominated by high concentrations in the $PM_{2.5}$ (and smaller) size range (i.e. East Asia). Moreover, nitrate aerosols over the Sahara are exclusively associated with dust particles which have a relatively high imaginary part of the refractive index, with typical values for SW wavelengths being ~0.005 (Di Biagio et al., 2019). As a result nitrate aerosols over the Sahara exhibit relatively strong absorption in the SW spectrum as well, and the combination of the bright surface of the desert below leads to a weakened cooling effect and even sometimes in localized warming. On the other hand, the RE_{ari} of fine NO_3^- particles due to interactions with LW radiation is negligible (Fig. 2iv), while its effect on SW radiation is about an order of magnitude smaller than that induced by the coarse NO_3^- aerosols (Fig. 2vi). The cooling induced by fine NO_3^- aerosols from the scattering of SW radiation is stronger over regions of high anthropogenic activity, namely the East Asian and Indian regions, which are characterized by high concentrations of fine NO_3^- aerosols, and peaks over eastern China (-0.25 W/m^2). Conversely, a weak warming effect (+0.15 W/m^2) is calculated over deserts (e.g. Gobi, Sahara) and volcanoes (e.g. Hawaii and Papua New Guinea).

3.2 Comparison of RE_{ari} Estimates by Sensitivity Cases.

The comparison of the calculated total NO_3^- radiative effect due to interactions with net, LW, and SW radiation for the sensitivity cases listed in Table 1 can be found in Table 2, which shows each of the estimates. Consideration of nitrate interactions with mineral dust cations can greatly affect the NO_3^- RE_{ari} estimates. Assuming that mineral dust particles are inert, the estimated warming due to LW radiation interactions is 52% weaker than in the base case where dust reactivity is considered. Similarly, the cooling effect exerted by nitrate aerosols through interactions with SW radiation is estimated to be 41% weaker under the assumption that mineral dust is non-reactive. Both estimates are lower when mineral dust is assumed to be chemically inert, since HNO_3 is no longer effectively adsorbed on dust particles and therefore the RE_{ari} by coarse NO_3^- aerosol is significantly weaker compared to the base case where it dominates the total NO_3^- effect (see Sect. 3.1). However, since both the estimated warming and cooling are weaker, the effects partially cancel each other out, resulting in a net cooling effect (-0.09 W/m^2) that is 18% weaker compared to the base case calculations. Assuming a homogeneous ionic composition for the dust, results simultaneously in both estimates for SW cooling and LW warming being 21% and 22% lower, respectively, weakening the estimate for the net cooling RE_{ari} by 18% (-0.09 W/m^2). The net direct radiative effect of total NO_3^- is the same for the cases where dust is assumed to have a homogeneous chemical composition and where it has no chemical identity, indicating the importance of both aspects for the impact of dust-nitrate interactions on the direct radiative effect. In the Half Dust scenario, the LW warming estimate is 17% weaker than in the base case, while the SW estimate is even more so (21%), resulting in a lower net cooling estimate of -0.08 W/m^2.

Finally, the Increased Dust scenario shows the strongest LW warming effect (17% increase over the base case) due to an increase in coarse mode nitrate. At the same time, the cooling effect due to interactions with SW radiation shows a smaller increase of 9%.. Thus, accounting for the historical increase in mineral dust emissions results in a net cooling estimate of -0.10 W/m^2, which is smaller than the base case. Interestingly, the behavior of the global total NO_3^- RE_{ari} does not exhibit linearity with respect to the global dust load. This is not surprising since the nitrate-dust interactions themselves are not linearly correlated, and a given increase or decrease in dust emissions does not lead to an analogous change in nitrate aerosol levels. For example, Karydis et al. (2016) have shown that moving from a scenario in which nitrate-dust chemistry is not considered to one in which it is, but with half dust emissions, resulted in a 39% increase in the tropospheric burden of nitrate aerosols. However, moving from a scenario with half to full dust emissions, the corresponding increase was only 9%. In our case, moving from the chemically inert dust scenario to the half dust scenario led to an 18% increase in atmospheric nitrate aerosol burden, while moving from the half dust scenario to the base case led to an additional 8% increase, and finally moving from the base case to the increased dust scenario led to an even smaller increase of 5%.

4 Radiative Effect from Aerosol-Cloud Interactions (RE_{aci})

4.1 Base Case

The global average RE_{aci} of total NO_3^- aerosols at the top of the atmosphere was found to be +0.17 W/m^2. In contrast, an estimate of the RE_{aci} of nitrate aerosols by Xu and Penner (2012) showed only a trivial cooling effect for particulate NO_3^- (-0.01 W/m^2). Similar to the RE_{ari}, the net RE_{aci} estimated by EMAC is driven by the effect on the SW part of the spectrum, which causes a warming effect of +0.27 W/m^2, while the effect on the LW radiation causes an average cooling of -0.10 W/m^2 (Table 3). Overall, the net RE_{aci} of total NO_3^- aerosols is reversed compared to the net RE_{ari}, i.e. RE_{aci} exerts a strong cooling effect over regions where RE_{ari} exerts a warming effect and vice versa (Fig. 3i). The reason for this is that the regions contributing to a cooling RE_{ari} are dominated by smaller sized nitrate aerosols and vice versa. Therefore, the size characteristics of the dominant nitrate aerosol population lead to different effects on the cloud optical properties as discussed in section 1. For example, as the dominance of smaller nitrate aerosols decreases over a particular region, the optical thinning of low-level clouds will have an opposite effect on the RE_{aci} (Fig. 1d). Details of the mechanism by which nitrate-dust interactions affect cloud microphysical processes are discussed in section 5. Over North America and Europe, RE_{aci} causes a warming effect of up to +3 W/m^2, driven solely by the effect on SW radiation (Fig. 3iii). Over the regions of East Asia and the Amazon and Congo basins, RE_{aci} reaches a maximum of +5 W/m^2, driven by both the effect on the SW (up to +4 W/m^2) and LW (up to +1.5 W/m^2) parts of the radiation spectrum. The cooling effect of RE_{aci} (up to -2 W/m^2) extends mainly between the equatorial line and the Tropic of Cancer, mainly due to the interaction of nitrate aerosols with desert dust particles (e.g. from the Sahara) and their effect on the terrestrial spectrum (LW) (Figs. 1c & 3ii). The cooling effect of dust interactions with anthropogenic particles in the LW spectrum corroborates the findings of Klingmüller et al. (2020) and is attributed to the reduced ice-water path due to the

depletion of small aerosols, which in turn leads to less trapped outgoing terrestrial radiation. In addition, Kok et al. (2023) note how the presence of dust particles leads to an optical thinning of cirrus clouds by reducing the number of ice crystals while increasing their size, which also leads to less trapping of outgoing LW radiation and thus a cooling effect (Fig. 1c). On the other hand, the warming effect of dust interactions with anthropogenic particles in the SW spectrum requires further investigation and is therefore discussed in more detail in Section 5.

4.2 Comparison of RE_{aci} Estimates by Sensitivity Cases.

Table 3 shows the comparison of the net, LW, and SW contributions of total NO_3^- to the RE_{aci} at the top of the atmosphere as calculated by the base case simulation and all sensitivity cases considered. By assuming a chemically inert dust, the calculated net RE_{aci} of nitrate decreases by 35%, resulting in a net warming of +0.11 W/m^2. As with the RE_{ari} estimate, this sensitivity case produces the largest deviation from the base case among all sensitivity simulations, for both the SW (37% less warming) and LW (40% less cooling) estimates. This is due to the fact that the absence of dust-nitrate interactions does not have such a large impact on the population of both aerosols and activated particles (see also Section 5). The assumption of a homogeneous ionic composition of the mineral dust leads to a weakened LW cooling estimate of 10% and a weakened SW warming estimate of 19% resulting in a net NO_3^- RE_{aci} of +0.13 W/m^2 (24% lower than in the base case). The reduced dust emissions result in a 15% weaker warming in the SW spectrum and a 20% weaker cooling in the LW spectrum, leading to an overall NO_3^- RE_{aci} of +0.15 W/m^2 (12% weaker than the base case scenario). This is because the reduced loading of nitrate aerosols, especially in the coarse mode, in the half dust scenario results in less absorption of LW radiation (Fig. 1c) (hence less cooling). Similarly, the effect of dust-nitrate interactions on the activation of smaller particles (Fig. 1d) is less drastic and results in a weaker inhibition of SW radiation scattering (hence less warming, see also Section 5). Finally, increased dust emissions in the increased dust scenario show a 10% increase in the LW cooling and an 8% decrease in the SW warming effect, surprisingly resulting in a net warming (+0.14 W/m^2) that is lower than in the half dust scenario. The reason that this scenario results in more LW cooling than the base case is that the increased amount of dust particles leads to even more optical thinning of the ice clouds, and therefore even less trapping of LW radiation (more cooling). However, the reason why the SW warming estimate is lower than the base case is more complicated. First, the transition from the half dust scenario to the base case and then to the increased dust scenario does not lead to an analogous increase in the nitrate aerosol burden (see Section 3.2). Moreover, since the number of aerosols has increased from the increased dust scenario to the base case, but the relative humidity has remained largely the same, there is more competition for water vapor because it is now distributed over a larger population. As a result, the wet radius increase in the presence of nitrates is not as strong in the increased dust scenario compared to the base case, and the depletion of smaller sized particles is also not as strong (not shown). The implications of the depletion of the aerosol population in the presence of nitrate aerosols on the microphysical processes of warm clouds, and consequently on the SW warming, are discussed in the next section.

5 Effect Of NO_3^- Aerosols on Cloud Microphysics

5.1 Maximum Supersaturation, Hygroscopicity and Wet Radius

To further investigate the cause of the positive RE_{aci} induced by the NO_3^- aerosols, their effect on the characteristics of the aerosol population as well as on the cloud microphysics is investigated, with respect to the lowest forming cloud level of 940 hPa. For this purpose, a sensitivity simulation is performed assuming a 'nitrate aerosol free' (NAF) atmosphere, in which the formation of NO_3^- aerosols has been switched off, but an advanced cloud scheme is considered. This simulation is used to determine whether the presence of NO_3^- aerosols has a significant effect on the hygroscopicity and size of atmospheric aerosols and ultimately on the maximum supersaturation developed during cloud formation. Over polluted areas affected by transported dust air masses from surrounding arid areas, the presence of NO_3^- aerosols can increase the CCN activity of the large mineral dust particles, resulting in a reduction of the maximum supersaturation and inhibiting the activation of the small anthropogenic particles into cloud droplets (Klingmüller et al., 2020). Results from the NAF sensitivity simulation support this hypothesis over parts of Eastern and Central Asia, where the maximum supersaturation decreases by up to 0.05%. In contrast, the presence of NO_3^- aerosols increases maximum supersaturation by up to 0.2% over North America, Europe, the Middle East, and parts of southern Asia (Fig. 4ii). Therefore, changes in maximum supersaturation caused by the presence of NO_3^- aerosols cannot explain their warming effect through the RE_{aci}. The presence of NO_3^- has a significant effect on the hygroscopicity of both fine and coarse aerosols and consequently on their wet radius, as shown in Figures 1a,b & 4. This is most evident for coarse desert dust particles, which mix with NO_3^- aerosols from urban and forest regions, increasing their hygroscopicity by an order of magnitude (up to 0.1), especially over the African-Asian dust belt and the Atacama Desert in South America (Fig. 4vi). Aerosol hygroscopicity is similarly increased for the fine mode particles both near arid regions and over the highly industrialized region of Southeast Asia (Fig. 4iv). On the other hand, the aerosol hygroscopicity for the two size modes is only slightly reduced, by up to 0.06 (or <10%) over the oceans and coasts of Europe and East Asia, due to interactions of NO_3^- with sea salt particles, reducing their hygroscopicity. The increased ability of both coarse dust aerosols and smaller aerosols to absorb water leads to an increase in their wet radius, but in different parts of the world. For example, fine particle sizes increase by up to 0.04 μm (up to 40%) mostly over regions of high anthropogenic activity (North America, Europe, and East Asia) (Fig. 4viii). On the other hand, coarse mode particle sizes are increased by up to 0.1 μm (up to 10%) over the forests of central Africa and the African-Asian dust belt zone (Fig. 4x), while showing a similar decrease near the coasts of the polluted northern hemisphere due to the effect of NO_3^- on the hygroscopicity of sea salt.

5.2 Number Concentrations of Aerosol and Activated Particles.

Figure 5 shows the effect of NO_3^- on the number concentration of fine and coarse aerosols between the base case and the 'NAF' sensitivity simulation, as well as the total aerosol population. The presence of NO_3^- aerosols decreases the total aerosol number concentration over forests and polluted regions (see also Fig. 1d). This behavior is driven solely by the decrease in smaller particle sizes, as the effect is minimal for the coarser particles (Figs. 5ii & 5iv). The largest decrease is

calculated over East and South Asia (up to 1000 cm^{-3} or 10%), while decreases of up to 200 cm^{-3} on average (~10%) are found over Europe, the USA, and Central Africa. This effect is directly related to the increased wet radius of the aerosol population (Fig. 4viii) over these regions and thus to its depositional efficiency. In addition, coarse dust particles become more hygroscopic due to interactions with NO_3^- aerosols that increase in size, resulting in increased coagulation with the smaller anthropogenic particles, which reduces their abundance. Similar interactions between dust and anthropogenic pollution aerosols were found by Klingmüller et al. (2020). The reduced aerosol number concentration in the presence of NO_3^- can lead to a reduction of particles that are also activated into cloud droplets. Such behavior can be seen in Figure 6, which shows the effect of NO_3^- on the number concentration of activated fine and coarse particles in cloud droplets between the base case and the 'NAF' sensitivity simulation. The reduction in the total number of activated cloud droplets is almost entirely due to the reduction in smaller size particles (Figs. 6ii & 6iv). A reduction in the total number of activated droplets of up to 30 cm^{-3} or 10% is observed over the USA, Amazon, Europe, Central Africa, and parts of the Middle East, while this reduction reaches up to 100 cm^{-3} (10%) over Southeast Asia, where the largest reductions in aerosol numbers are also calculated (Fig. 4ii). In turn, these are the regions where the warming effect of NO_3^- aerosols on the calculated mean RE_{aci} is strongest (Figure 3i). The small increase in activated droplets (~ 10 cm^{-3} or 1%) over Beijing, which concerns the fine mode particles, is most likely because their number concentration decreases with increasing size. The high aerosol number concentration there, which is the global maximum (Figure 5i), results in a hotspot of more readily activated particles in the presence of NO_3^-. On the other hand, the CDNC decreases slightly over the Sahara due to the more efficient deposition capacity of coarse dust particles due to their interactions with nitrate aerosols, which is also reflected in the decrease in aerosol number (Fig. 6iv). Overall, the lower particle number in the presence of NO_3^- aerosols hinders the ability of the smaller anthropogenic particles to activate into cloud droplets, leading to a reduced cloud cover and thus a reduced cloud albedo effect, similar to the findings of Klingmüller et al. (2020). Therefore, not only less LW radiation is absorbed, but more importantly, less SW radiation is scattered back to space, resulting in an overall warming of the net average RE_{aci} for total NO_3^- aerosols.

6. Conclusions and Discussion

This study presents the effects of interactions between mineral dust and NO_3^- aerosols on the present global TOA radiative effect of the latter. We investigate how the presence of dust affects the radiative effect of NO_3^- aerosols, both through aerosol interactions with radiation and separately with clouds (RE_{ari} and RE_{aci}, respectively). Sensitivity simulations are also performed, varying both the mineral dust composition and its emissions, to assess their effect on the calculated NO_3^- aerosol radiative effect.

It was found that the global average net RE_{ari} of total NO_3^- aerosols is -0.11 W/m^2, which is mainly due to the cooling from the shortwave part of the radiation spectrum due to scattering, equal to -0.34 W/m^2. A warming from the longwave part of the spectrum due to absorption was found to be +0.23 W/m^2 on global average and was mainly located over regions with high concentrations of coarse NO_3^- aerosols. SW cooling was also observed in these regions, but also

over regions of high anthropogenic activity, mainly over the polluted northern hemisphere. The overall sign of the net RE_{ari} for total NO_3^- aerosols was dominated by the behavior of the coarse mode particles, which contributed on average -0.09 W/m^2. Specifically, coarse nitrate particles were responsible for 82% of the net cooling and 100% of the net warming, while the fine mode played a minor role. The sensitivity experiments revealed that the chemistry of the mineral dust is the most important factor in changing the estimated RE_{ari} of the total NO_3^- aerosols. In particular, the LW warming is most affected by this assumption, being 52% weaker after assuming chemically inert dust emissions, while the SW cooling is reduced by 41% compared to the base case simulation, amounting to a net cooling of -0.09 W/m^2. A globally homogeneous ionic composition for mineral dust had a smaller effect in LW (22% decrease) and SW (21% decrease) but resulted in the same net estimate of -0.09 W/m^2. Halving the dust emissions resulted in weaker estimates for LW and SW by 17% and 21%, respectively, and the lowest overall net RE_{ari} of -0.08 W/m^2. On the other hand, a 50% increase in dust emissions increased both LW warming and SW cooling by 17% and 9% respectively, resulting in a net cooling RE_{ari} of -0.01 W/m^2, indicating the strong non-linear relationship of nitrate-dust interactions and how they affect the radiative effect estimates.

The global average net RE_{aci} of total NO_3^- aerosols was +0.17 W/m^2 due to the effect on the shortwave portion of the spectrum. This was found to be +0.27 W/m^2, while the cooling from the longwave part was -0.10 W/m^2. Spatially, the net RE_{aci} is reversed compared to the net RE_{ari} for total NO_3^- aerosols, where regions responsible for a strong SW cooling of the RE_{ari} contribute to a strong SW warming of the RE_{aci} and vice versa. This is due to the fact that nitrate-dust interactions challenge the dominance of smaller particles over heavily polluted regions, reducing the reflectivity of warm cloud and thus having an opposite effect on the RE_{aci}. The sensitivity experiments again showed that the consideration of the chemistry of the mineral dust is important for the calculation of the RE_{aci} of the total NO_3^- aerosols. When the dust was assumed to be chemically inert, the LW and SW estimates were up to 40% weaker, resulting in a warming of +0.11 W/m^2. Assuming a homogeneous ion composition resulted in a smaller weakening of the estimates (up to 18%) and a net warming of +0.13 W/m^2. When dust emissions were halved, the LW cooling was reduced slightly more than in the base case, resulting in a net warming of +0.15 W/m^2. The 50% increase in dust emissions had the largest effect on LW behavior (10% increase), but surprisingly the net estimate (+0.14 W/m^2) was smaller than in the half-dust scenario. The reason for this is that the SW estimate did not increase, but decreased by 8% due to the fact that in this scenario the increased nitrate burden causes increased competition for the available supersaturation and the effect of dust-nitrate interactions on the smaller aerosol populations is not as emphasized as in the base case.

The total NO_3^- aerosol RE_{aci} shows a positive sign, which is attributed to a reduced cloud albedo effect. More specifically, although the presence or absence of NO_3^- aerosol in the atmosphere did not significantly affect the total available maximum supersaturation, it did alter both the hygroscopicity and wet radii of the aerosols. In the presence of NO_3^-, the hygroscopicity of aerosols over deserts was increased by up to an order of magnitude, leading to an increase in their wet radius of up to 10%, with an even larger increase of up to 40% for smaller particles over urban regions. Therefore, in the presence of NO_3^- aerosols, there is an increased depletion of fine particles by coagulation with coarser particles (i.e. mineral dust) that have been further increased in size.

The reduction in the number of aerosols is as much as 10% in some regions, with maximum reductions calculated over Southeast Asia. This reduction in the number of fine aerosols leads to a reduction in the number of cloud droplets activated by fine aerosols (also up to 10%), which would otherwise have absorbed more outgoing longwave radiation and, more importantly, scattered more incoming shortwave radiation. Thus, the reduced cloud albedo effect leads to a cooling in the longwave part of the spectrum, which is offset by a strong warming in the shortwave part.

REFERENCES

Albrecht, B. A.: Aerosols, Cloud Microphysics, and Fractional Cloudiness, Science, 245(4923), 1227-1230, https://doi.org/10.1126/science.245.4923.1227 , 1989.

Arias, P.A., N. Bellouin, E. Coppola, R.G. Jones, G. Krinner, J. Marotzke, V. Naik, M.D. Palmer, G.-K. Plattner, J. Rogelj, M. Rojas, J. Sillmann, T. Storelvmo, P.W. Thorne, B. Trewin, K. Achuta Rao, B. Adhikary, R.P. Allan, K. Armour, G. Bala, R. Barimalala, S. Berger, J.G. Canadell, C. Cassou, A. Cherchi, W. Collins, W.D. Collins, S.L. Connors, S. Corti, F. Cruz, F.J. Dentener, C. Dereczynski, A. Di Luca, A. Diongue Niang, F.J. Doblas-Reyes, A. Dosio, H. Douville, F. Engelbrecht, V. Eyring, E. Fischer, P. Forster, B. Fox-Kemper, J.S. Fuglestvedt, J.C. Fyfe, N.P. Gillett, L. Goldfarb, I. Gorodetskaya, J.M. Gutierrez, R. Hamdi, E. Hawkins, H.T. Hewitt, P. Hope, A.S. Islam, C. Jones, D.S. Kaufman, R.E. Kopp, Y. Kosaka, J. Kossin, S. Krakovska, J.-Y. Lee, J. Li, T. Mauritsen, T.K. Maycock, M. Meinshausen, S.-K. Min, P.M.S. Monteiro, T. Ngo-Duc, F. Otto, I. Pinto, A. Pirani, K. Raghavan, R. Ranasinghe, A.C. Ruane, L. Ruiz, J.-B. Sallée, B.H. Samset, S. Sathyendranath, S.I. Seneviratne, A.A. Sörensson, S. Szopa, I. Takayabu, A.-M. Tréguier, B. van den Hurk, R. Vautard, K. von Schuckmann, S. Zaehle, X. Zhang, and K. Zickfeld, 2021: Technical Summary. In *Climate Change 2021: The Physical Science Basis. Contribution of Working Group I to the Sixth Assessment Report of the Intergovernmental Panel on Climate Change* [Masson-Delmotte, V., P. Zhai, A. Pirani, S.L. Connors, C. Péan, S. Berger, N. Caud, Y. Chen, L. Goldfarb, M.I. Gomis, M. Huang, K. Leitzell, E. Lonnoy, J.B.R. Matthews, T.K. Maycock, T. Waterfield, O. Yelekçi, R. Yu, and B. Zhou (eds.)]. Cambridge University Press, Cambridge, United Kingdom and New York, NY, USA, https://doi.org/10.1017/9781009157896.002 , 2021.

Astitha, M., Lelieveld, J., Kader, M. A., Pozzer, A., and de Meij, A.: Parameterization of dust emissions in the global atmospheric chemistry-climate model EMAC: impact of nudging and soil properties, Atmospheric Chemistry and Physics , 12(22), 11057-11083, https://doi.org/10.5194/acp-12-11057-2012 , 2012.

Bacer, S., Sullivan, S. C., Karydis, V. A., Barahona, D., Kramer, M., Nenes, A., Tost, H., Tsimpidi, A. P., Lelieveld, J., and Pozzer, A.: Implementation of a comprehensive ice crystal formation parameterization for cirrus and mixed-phase clouds in the EMAC model (based on MESSy 2.53), Geoscientific Model Development , 11(10), https://doi.org/10.5194/gmd-11-4021-2018 , 2018.

Barahona, D. and Nenes, A.: Parameterizing the competition between homogeneous and heterogeneous freezing in cirrus cloud formation - monodisperse ice nuclei, Atmospheric Chemistry and Physics , 9(16), 369-381, https://doi.org/10.5194/acp-9-5933-2009 , 2009.

Barahona, D., West, R., Stier, P., Romakkaniemi, S., Kokkola, H., and Nenes, A.: Comprehensively accounting for the effect of giant CCN in cloud activation parameterizations, Atmospheric Chemistry and Physics , 10(5) , 2467-2473, https://doi.org/10.5194/acp-10-2467-2010 , 2010.

Bauer, S. E., Koch, D., Unger, N., Metzger, S. M., Shindell, D. T., and Streets, D. G.: Nitrate aerosols today and in 2030: a global simulation including aerosols and tropospheric ozone, Atmospheric Chemistry and Physics , 7(19) , https://doi.org/10.5194/acp-7-5043-2007 , 2007a.

Bauer, S. E., Mishchenko, M. I., Lacis, A. A., Zhang, S., Perlwitz, J., and Metzger, S. M.: Do sulfate and nitrate coatings on mineral dust have important effects on radiative properties and climate modeling?, Journal of Geophysical Research: Atmospheres, 112(D6), https://doi.org/10.1029/2005JD006977, 2007b.

Bellouin, N., Rae, J., Jones, A., Johnson, C., Haywood, J., and Boucher, O.: Aerosol forcing in the Climate Model Intercomparison Project (CMIP5) simulations by HadGEM2-ES and the role of ammonium nitrate, Journal of Geophysical Research: Atmospheres, 116(D20) , https://doi.org/10.1029/2011JD016074 , 2011.

Bond, T. C. and Bergstrom, R. W.: Light absorption by carbonaceous particles: An investigative review, Aerosol Science and Technology, 40(1), 27-67, https://doi.org/10.1080/02786820500421521 , 2006.

Bouwman, A. F., Lee, D. S., Asman, W. A. H., Dentener, F. J., VanderHoek, K. W., and Olivier, J. G. J.: A global high-resolution emission inventory for ammonia, Global Biogeochemical Cycles , 11(4) , https://doi.org/10.1029/97GB02266 , 1997.

Dentener, F., Kinne, S., Bond, T., Boucher, O., Cofala, J., Generoso, S., Ginoux, P., Gong, S., Hoelzemann, J. J., Ito, A., Marelli, L., Penner, J. E., Putaud, J. P., Textor, C., Schulz, M., van der Werf, G. R., and Wilson, J.: Emissions of primary aerosol and precursor gases in the years 2000 and 1750 prescribed data-sets for AeroCom, Atmospheric Chemistry and Physics , 6(12) , 4321-4344, https://doi.org/10.5194/acp-6-4321-2006 , 2006.

Di Biagio, C., Formenti, P., Balkanski, Y., Caponi, L., Cazaunau, M., Pangui, E., Journet, E., Nowak, S., Andreae, M. O., Kandler, K., Saeed, T., Piketh, S., Seibert, D., Williams, E., and Doussin, J. F.: Complex refractive indices and single-scattering albedo of global dust aerosols in the shortwave spectrum and relationship to size and iron content, Atmospheric Chemistry and Phys., 19(24), 15503-15531, https://doi.org/10.5194/acp-19-15503-2019 , 2019.

Dietmuller, S., Jockel, P., Tost, H., Kunze, M., Gellhorn, C., Brinkop, S., Fromming, C., Ponater, M., Steil, B., Lauer, A., and Hendricks, J.: A new radiation infrastructure for the Modular Earth Submodel System (MESSy, based on version 2.51), Geoscientific Model Development, 9(6) , 2209-2222, https://doi.org/10.5194/gmd-9-2209-2016 , 2016.

Fan, S.-M., Horowitz, L. W., Levy Ii, H., and Moxim, W. J.: Impact of air pollution on wet deposition of mineral dust aerosols, Geophysical Research Letters, 31(2), https://doi.org/10.1029/2003GL018501 , 2004.

Fuchs, N. A. and Davies, C. N.: The mechanics of aerosols, Pergamon Press, Oxford, ISBN 9780486660554, 1964.

Gao, M., Ji, D., Liang, F., and Liu, Y.: Attribution of aerosol direct radiative forcing in China and India to emitting sectors, Atmospheric Environment, 190, 35-42, https://doi.org/10.1016/j.atmosenv.2018.07.011 , 2018.

Ghan, S. J., Liu, X., Easter, R. C., Zaveri, R., Rasch, P. J., Yoon, J. H., and Eaton, B.: Toward a Minimal Representation of Aerosols in Climate Models: Comparative Decomposition of Aerosol Direct, Semidirect, and Indirect Radiative Forcing, Journal of Climate, 25(19), 6461-6476, https://doi.org/10.1175/JCLI-D-11-00650.1, 2012.

Grewe, V., Brunner, D., Dameris, M., Grenfell, J. L., Hein, R., Shindell, D., and Staehelin, J.: Origin and variability of upper tropospheric nitrogen oxides and ozone at northern mid-latitudes, Atmospheric Environment, 35(20), 3421-3433, https://doi.org/10.1016/S1352-2310(01)00134-0 , 2001.

Hauglustaine, D. A., Balkanski, Y., and Schulz, M.: A global model simulation of present and future nitrate aerosols and their direct radiative forcing of climate, Atmospheric Chemistry and Physics, 14(20), 11031-11063, https://doi.org/10.5194/acp-14-11031-2014 , 2014.

IPCC, 2013: *Climate Change 2013:* The Physical Science Basis. Contribution of Working Group I to the Fifth Assessment Report of the Intergovernmental Panel on Climate Change [Stocker, T.F., D. Qin, G.-K. Plattner, M. Tignor, S.K. Allen, J. Boschung, A. Nauels, Y. Xia, V. Bex and P.M. Midgley (eds.)]. Cambridge University Press, Cambridge, United Kingdom and New York, NY, USA.

Jockel, P., Sander, R., Kerkweg, A., Tost, H., and Lelieveld, J.: Technical note: The Modular Earth Submodel System (MESSy) - a new approach towards Earth System Modeling, Atmos Chem Phys, 5(2), 433-444, https://doi.org/10.5194/acp-5-433-2005 , 2005.

Jockel, P., Tost, H., Pozzer, A., Bruhl, C., Buchholz, J., Ganzeveld, L., Hoor, P., Kerkweg, A., Lawrence, M. G., Sander, R., Steil, B., Stiller, G., Tanarhte, M., Taraborrelli, D., Van Aardenne, J., and Lelieveld, J.: The atmospheric chemistry general circulation model ECHAM5/MESSy1: consistent simulation of ozone from the surface to the mesosphere, Atmospheric Chemistry and Physics, 6(12), 5067-5104, https://doi.org/10.5194/acp-6-5067-2006 , 2006.

Kakavas, S., Pandis, S. N., and Nenes, A.: ISORROPIA-Lite: A Comprehensive Atmospheric Aerosol Thermodynamics Module for Earth System Models, Tellus Series B-Chemical and Physical Meteorology, 74(1), 1-23, https://doi.org/10.16993/tellusb.33 , 2022.

Kanakidou, M., Seinfeld, J. H., Pandis, S. N., Barnes, I., Dentener, F. J., Facchini, M. C., Van Dingenen, R., Ervens, B., Nenes, A., Nielsen, C. J., Swietlicki, E., Putaud, J. P., Balkanski, Y., Fuzzi, S., Horth, J., Moortgat, G. K., Winterhalter, R., Myhre, C. E. L., Tsigaridis, K., Vignati, E., Stephanou, E. G., and Wilson, J.: Organic aerosol and global climate modelling: a review, Atmospheric Chemistry and Physics, 5(4), 1053-1123, https://doi.org/10.5194/acp-5-1053-2005 , 2005.

Karydis, V. A., Kumar, P., Barahona, D., Sokolik, I. N., and Nenes, A.: On the effect of dust particles on global cloud condensation nuclei and cloud droplet number, Journal of Geophysical Research: Atmospheres, 116, https://doi.org/10.1029/2011JD016283, 2011.

Karydis, V. A., Tsimpidi, A. P., Pozzer, A., Astitha, M., and Lelieveld, J.: Effects of mineral dust on global atmospheric nitrate concentrations, Atmospheric Chemistry and Physics, 16(3), 1491-1509, https://doi.org/10.5194/acp-16-1491-2016 , 2016.

Karydis, V. A., Tsimpidi, A. P., Bacer, S., Pozzer, A., Nenes, A., and Lelieveld, J.: Global impact of mineral dust on cloud droplet number concentration, Atmospheric Chemistry and Physics, 17(9), 5601-5621, https://doi.org/10.5194/acp-17-5601-2017 , 2017.

Kelly, J. T., Chuang, C. C., and Wexler, A. S.: Influence of dust composition on cloud droplet formation, Atmospheric Environment, 41(14), 2904-2916, https://doi.org/10.1016/j.atmosenv.2006.12.008 , 2007.

Kerkweg, A., Buchholz, J., Ganzeveld, L., Pozzer, A., Tost, H., and Jockel, P.: Technical note: An implementation of the dry removal processes DRY DEPosition and SEDImentation in the modular earth submodel system (MESSy), Atmospheric Chemistry and Physics, 6(12), 4617-4632, https://doi.org/10.5194/acp-6-4617-2006 , 2006.

Khain, A. P. and Pinsky, M.: Physical Processes in Clouds and Cloud Modeling, Cambridge University Press, ISBN 9781139049481, 2018.

Kirchstetter, T. W., Novakov, T., and Hobbs, P. V.: Evidence that the spectral dependence of light absorption by aerosols is affected by organic carbon, Journal of Geophysical Research: Atmospheres, 109(D21), https://doi.org/10.1029/2004JD004999 , 2004.

Klingmüller, K., Metzger, S., Abdelkader, M., Karydis, V. A., Stenchikov, G. L., Pozzer, A., and Lelieveld, J.: Revised mineral dust emissions in the atmospheric chemistry-climate model EMAC (MESSy 2.52 DU_Astitha1 KKDU2017 patch), Geoscientific Model Development, 11(3), 989-1008, https://doi.org/10.5194/gmd-11-989-2018 , 2018.

Klingmüller, K., Lelieveld, J., Karydis, V. A., and Stenchikov, G. L.: Direct radiative effect of dust–pollution interactions, Atmospheric Chemistry and Physics, 19(11), 7397-7408, https://doi.org/10.5194/acp-19-7397-2019 , 2019.

Klingmüller, K., Karydis, V. A., Bacer, S., Stenchikov, G. L., and Lelieveld, J.: Weaker cooling by aerosols due to dust–pollution interactions, Atmospheric Chemistry and Physics, 20(23), 15285-15295, https://doi.org/10.5194/acp-20-15285-2020 , 2020.

Kok, J. F., Storelvmo, T., Karydis, V. A., Adebiyi, A. A., Mahowald, N. M., Evan, A. T., He, C., and Leung, D. M.: Mineral dust aerosol impacts on global climate and climate change, Nature Reviews Earth & Environment, 4(2), 71-86, https://doi.org/10.1038/s43017-022-00379-5 , 2023.

Lance, S., Nenes, A., and Rissman, T. A.: Chemical and dynamical effects on cloud droplet number: Implications for estimates of the aerosol indirect effect, Journal of Geophysical Research: Atmospheres, 109(D22), https://doi.org/10.1029/2004JD004596 , 2004.

Laskin, A., Wietsma, T. W., Krueger, B. J., and Grassian, V. H.: Heterogeneous chemistry of individual mineral dust particles with nitric acid: A combined CCSEM/EDX, ESEM, and ICP-MS study, Journal of Geophysical Research: Atmospheres, 110(D10), https://doi.org/10.1029/2004JD005206 , 2005.

Li, J., Wang, W.-C., Liao, H., and Chang, W.: Past and future direct radiative forcing of nitrate aerosol in East Asia, Theoretical and Applied Climatology, 121, 445-458, https://doi.org/10.1007/s00704-014-1249-1 , 2015.

Liao, H., Seinfeld, J. H., Adams, P. J., and Mickley, L. J.: Global radiative forcing of coupled tropospheric ozone and aerosols in a unified general circulation model, Journal of Geophysical Research: Atmospheres, 109(D16), https://doi.org/10.1029/2003JD004456 , 2004.

Lohmann, U. and Roeckner, E.: Design and performance of a new cloud microphysics scheme developed for the ECHAM general circulation model, Climate Dynamics, 12, 557-572, https://doi.org/10.1007/BF00207939 , 1996.

Lohmann, U. and Feichter, J.: Global indirect aerosol effects: a review, Atmospheric Chemistry and Physics, 5(3), https://doi.org/10.5194/acp-5-715-2005 , 2005.

Lohmann, U. and Ferrachat, S.: Impact of parametric uncertainties on the present-day climate and on the anthropogenic aerosol effect, Atmospheric Chemistry and Physics, 10(23), https://doi.org/10.5194/acp-10-11373-2010 , 2010.

Milousis, A., Tsimpidi, A. P., Tost, H., Pandis, S. N., Nenes, A., Kiendler-Scharr, A., and Karydis, V. A.: Implementation of the ISORROPIA-lite aerosol thermodynamics model into the EMAC chemistry climate model (based on MESSy v2.55): implications for aerosol composition and acidity, Geoscientific Model Development, 17(3), 1111-1131, https://doi.org/10.5194/gmd-17-1111-2024 , 2024.

Morales Betancourt, R. and Nenes, A.: Understanding the contributions of aerosol properties and parameterization discrepancies to droplet number variability in a global climate model, Atmospheric Chemistry and Physics, 14(9), 4809-4826, https://doi.org/10.5194/acp-14-4809-2014 , 2014.

Myhre, G., Samset, B. H., Schulz, M., Balkanski, Y., Bauer, S., Berntsen, T. K., Bian, H., Bellouin, N., Chin, M., Diehl, T., Easter, R. C., Feichter, J., Ghan, S. J., Hauglustaine, D., Iversen, T., Kinne, S., Kirkevåg, A., Lamarque, J. F., Lin, G., Liu, X., Lund, M. T., Luo, G., Ma, X., van Noije, T., Penner, J. E., Rasch, P. J., Ruiz, A., Seland, Ø., Skeie, R. B., Stier, P., Takemura, T., Tsigaridis, K., Wang, P., Wang, Z., Xu, L., Yu, H., Yu, F., Yoon, J. H., Zhang, K., Zhang, H., and Zhou, C.: Radiative forcing of the direct aerosol effect from AeroCom Phase II simulations, Atmospheric Chemistry and Physics, 13(4), 1853-1877, https://doi.org/10.5194/acp-13-1853-2013 , 2013.

Myhre, G., Shindell, D., and Pongratz, J.: Anthropogenic and natural radiative forcing, Climate Change 2013-The Physical Science Basis, 659-740, https://dx.doi.org/10.1017/CBO9781107415324.018 , 2014.

Nenes, A., Murray, B., Bougiatioti, A. (2014). Mineral Dust and its Microphysical Interactions with Clouds. In: Knippertz, P., Stuut, JB. (eds) Mineral Dust. Springer, Dordrecht. https://doi.org/10.1007/978-94-017-8978-3_12 , 2014.

Pozzer, A., Jockel, P. J., Sander, R., Williams, J., Ganzeveld, L., and Lelieveld, J.: Technical note: the MESSy-submodel AIRSEA calculating the air-sea exchange of chemical species, Atmospheric Chemistry and Physics, 6(12), 5435-5444, https://doi.org/10.5194/acp-6-5435-2006 , 2006.

Pringle, K. J., Tost, H., Message, S., Steil, B., Giannadaki, D., Nenes, A., Fountoukis, C., Stier, P., Vignati, E., and Leieved, J.: Description and evaluation of GMXe: a new aerosol submodel for global simulations (v1), Geoscientific Model Development, 3(2), https://doi.org/10.5194/gmd-3-391-2010 , 2010a.

Pringle, K. J., Tost, H., Metzger, S., Steil, B., Giannadaki, D., Nenes, A., Fountoukis, C., Stier, P., Vignati, E., and Lelieveld, J.: Corrigendum to "Description and evaluation of GMXe: a new aerosol submodel for global simulations (v1)" published in Geosci. Model Dev., 3, 391–412, 2010, Geoscientific Model Development, 3(2), 413-413, https://doi.org/10.5194/gmd-3-413-2010 , 2010b.

Roeckner, E., Brokopf, R., Esch, M., Giorgetta, M., Hagemann, S., Kornblueh, L., Manzini, E., Schlese, U., and Schulzweida, U.: Sensitivity of simulated climate to horizontal and vertical resolution in the ECHAM5 atmosphere model, Journal of Climate, 19(16), 3771-3791, https://doi.org/10.1175/JCLI3824.1 , 2006.

Sander, R., Baumgaertner, A., Cabrera-Perez, D., Frank, F., Gromov, S., Grooss, J. U., Harder, H., Huijnen, V., Jockel, P., Karydis, V. A., Niemeyer, K. E., Pozzer, A., Hella, R. B., Schultz, M. G., Taraborrelli, D., and

Tauer, S.: The community atmospheric chemistry box model CAABA/MECCA-4.0, Geoscientific Model Development, 12(4), 1365-1385, https://doi.org/10.5194/gmd-12-1365-2019 , 2019.
Seinfeld, J. H. and Pandis, S. N.: Atmospheric chemistry and physics from air pollution to climate change, John Wiley & Sons, ISBN 1118947401, 2016.
Seinfeld, J. H., Bretherton, C., Carslaw, K. S., Coe, H., DeMott, P. J., Dunlea, E. J., Feingold, G., Ghan, S., Guenther, A. B., Kahn, R., Kraucunas, I., Kreidenweis, S. M., Molina, M. J., Nenes, A., Penner, J. E., Prather, K. A., Ramanathan, V., Ramaswamy, V., Rasch, P. J., Ravishankara, A. R., Rosenfeld, D., Stephens, G., and Wood, R.: Improving our fundamental understanding of the role of aerosol−cloud interactions in the climate system, Proceedings of the National Academy of Sciences, 113(21), 5781-5790, https://doi.org/10.1073/pnas.1514043113 , 2016.
Sposito, G.: The Chemistry of Soils, Oxford University Press, New York, ISBN 9780190630881, 1989.
Sundqvist, H., Berge, E., and Kristjánsson, J. E.: Condensation and Cloud Parameterization Studies with a Mesoscale Numerical Weather Prediction Model, Monthly Weather Review, 117(8), 1641-1657, https://doi.org/10.1175/1520-0493(1989)117%3C1641:CACPSW%3E2.0.CO;2 , 1989.
Tompkins, A. M.: A Prognostic Parameterization for the Subgrid-Scale Variability of Water Vapor and Clouds in Large-Scale Models and Its Use to Diagnose Cloud Cover, Journal of the Atmospheric Sciences, 59(12), 1917-1942, https://doi.org/10.1175/1520-0469(2002)059%3C1917:APPFTS%3E2.0.CO;2 , 2002.
Tost, H., Jockel, P. J., Kerkweg, A., Sander, R., and Lelieveld, J.: Technical note: A new comprehensive SCAVenging submodel for global atmospheric chemistry modelling, Atmospheric Chemistry and Physics, 6(3), 565-574, https://doi.org/10.5194/acp-6-565-2006 , 2006.
Tost, H., Jöckel, P., and Lelieveld, J.: Lightning and convection parameterisations - uncertainties in global modelling, Atmospheric Chemistry and Physics, 7(17), 4553-4568, https://doi.org/10.5194/acp-7-4553-2007 , 2007a.
Tost, H., Jockel, P., Kerkweg, A., Pozzer, A., Sander, R., and Lelieveld, J.: Global cloud and precipitation chemistry and wet deposition: tropospheric model simulations with ECHAM5/MESSy1, Atmospheric Chemistry and Physics, 7(10), 2733-2757, https://doi.org/10.5194/acp-7-2733-2007 , 2007b.
Trump, E. R., Fountoukis, C., Donahue, N. M., and Pandis, S. N.: Improvement of simulation of fine inorganic PM levels through better descriptions of coarse particle chemistry, Atmospheric Environment, 102, 274-281, https://doi.org/10.1016/j.atmosenv.2014.11.059 , 2015.
Tsigaridis, K. and Kanakidou, M.: The present and future of secondary organic aerosol direct forcing on climate, Current Climate Change Reports, 4, 84-98, https://doi.org/10.1007/s40641-018-0092-3 , 2018.
Twomey, S.: The Influence of Pollution on the Shortwave Albedo of Clouds, Journal of Atmospheric Sciences, 34, 1149-1152, https://doi.org/10.1175/1520-0469(1977)034%3C1149:TIOPOT%3E2.0.CO;2 , 1977.
Urdiales-Flores, D., Zittis, G., Hadjinicolaou, P., Osipov, S., Klingmüller, K., Mihalopoulos, N., Kanakidou, M., Economou, T., and Lelieveld, J.: Drivers of accelerated warming in Mediterranean climate-type regions, npj Climate and Atmospheric Science, 6(1), 97, https://doi.org/10.1038/s41612-023-00423-1 , 2023.
Vignati, E., Wilson, J., and Stier, P.: M7: An efficient size-resolved aerosol microphysics module for large-scale aerosol transport models, Journal of Geophysical Research: Atmospheres, 109(D22), https://doi.org/10.1029/2003JD004485 , 2004.
Wong, J. P. S., Tsagkaraki, M., Tsiodra, I., Mihalopoulos, N., Violaki, K., Kanakidou, M., Sciare, J., Nenes, A., and Weber, R. J.: Atmospheric evolution of molecular-weight-separated brown carbon from biomass burning, Atmospheric Chemistry and Physics, 19(11), 7319-7334, https://doi.org/10.5194/acp-19-7319-2019 , 2019.
Xu, L. and Penner, J. E.: Global simulations of nitrate and ammonium aerosols and their radiative effects, Atmospheric Chemistry and Physics, 12(20), https://doi.org/10.5194/acp-12-9479-2012 , 2012.
Yienger, J. J. and Levy, H.: EMPIRICAL-MODEL OF GLOBAL SOIL-BIOGENIC NOX EMISSIONS, Journal of Geophysical Research: Atmospheres, 100(D6), https://doi.org/10.1029/95JD00370 , 1995.

Zhang, Y., Forrister, H., Liu, J., Dibb, J., Anderson, B., Schwarz, J. P., Perring, A. E., Jimenez, J. L., Campuzano-Jost, P., Wang, Y., Nenes, A., and Weber, R. J.: Top-of-atmosphere radiative forcing affected by brown carbon in the upper troposphere, Nature Geoscience, 10(7), https://doi.org/10.1038/ngeo2960 , 2017.
Zhang, B.: The effect of aerosols to climate change and society, Journal of Geoscience and Environment Protection, 8(08), 55, https://doi.org/10.4236/gep.2020.88006 , 2020.

Table 1: Differences between base case and sensitivity simulations performed.

Simulation Name	Conditions Applied
Base Case	Mineral dust ion composition according to Karydis et al. (2016)
Sensitivity 1: Chemically Inert Dust	Mineral dust emitted exclusively as a chemically inert bulk particle
Sensitivity 2: Homogeneous Ion Composition	Global homogeneous ionic composition of mineral dust particles according to Sposito (1989)
Sensitivity 3: Half Dust Scenario	50% reduced dust emission flux.
Sensitivity 4: Increased Dust Scenario	50% increased dust emission flux.

Table 2: Net, longwave, and shortwave global mean TOA RE_{ari} of total, coarse, and fine NO_3^- aerosols for the base case and each sensitivity case simulations.

Simulation	Aerosol Component	TOA RE_{ari} (W/m^2)		
		Net	**LW**	**SW**
Base Case	Total NO_3^-	- 0.11	+ 0.23	- 0.34
	Coarse NO_3^-	- 0.09	+ 0.23	- 0.32
	Fine NO_3^-	- 0.02	~ 0	- 0.02
Chemically Inert Dust	Total NO_3^-	- 0.09	+ 0.11	- 0.20
	Coarse NO_3^-	- 0.07	+ 0.11	- 0.18
	Fine NO_3^-	- 0.02	~ 0	- 0.02
Homogeneous Ion Composition	Total NO_3^-	- 0.09	+ 0.18	- 0.27
	Coarse NO_3^-	- 0.08	+ 0.18	- 0.26
	Fine NO_3^-	- 0.01	~ 0	- 0.01
Half Dust Scenario	Total NO_3^-	- 0.08	+ 0.19	- 0.27
	Coarse NO_3^-	- 0.06	+ 0.19	- 0.25
	Fine NO_3^-	- 0.02	~ 0	- 0.02

Increased Dust Scenario	Total NO_3^-	- 0.10	+ 0.27	- 0.37
	Coarse NO_3^-	- 0.08	+ 0.27	- 0.35
	Fine NO_3^-	- 0.02	~ 0	- 0.02

Table 3: Net, longwave, and shortwave global mean TOA RE_{aci} of total NO_3^- aerosols for the base case and each sensitivity case simulations.

Simulation	**TOA RE_{aci} (W/m^2)**		
	Net	**LW**	**SW**
Base Case	+ 0.17	- 0.10	+ 0.27
Chemically Inert Dust	+ 0.11	- 0.06	+ 0.17
Homogeneous Ion Composition	+ 0.13	- 0.09	+ 0.22
Half Dust Scenario	+ 0.15	- 0.08	+ 0.23
Increased Dust Scenario	+ 0.14	- 0.11	+ 0.25

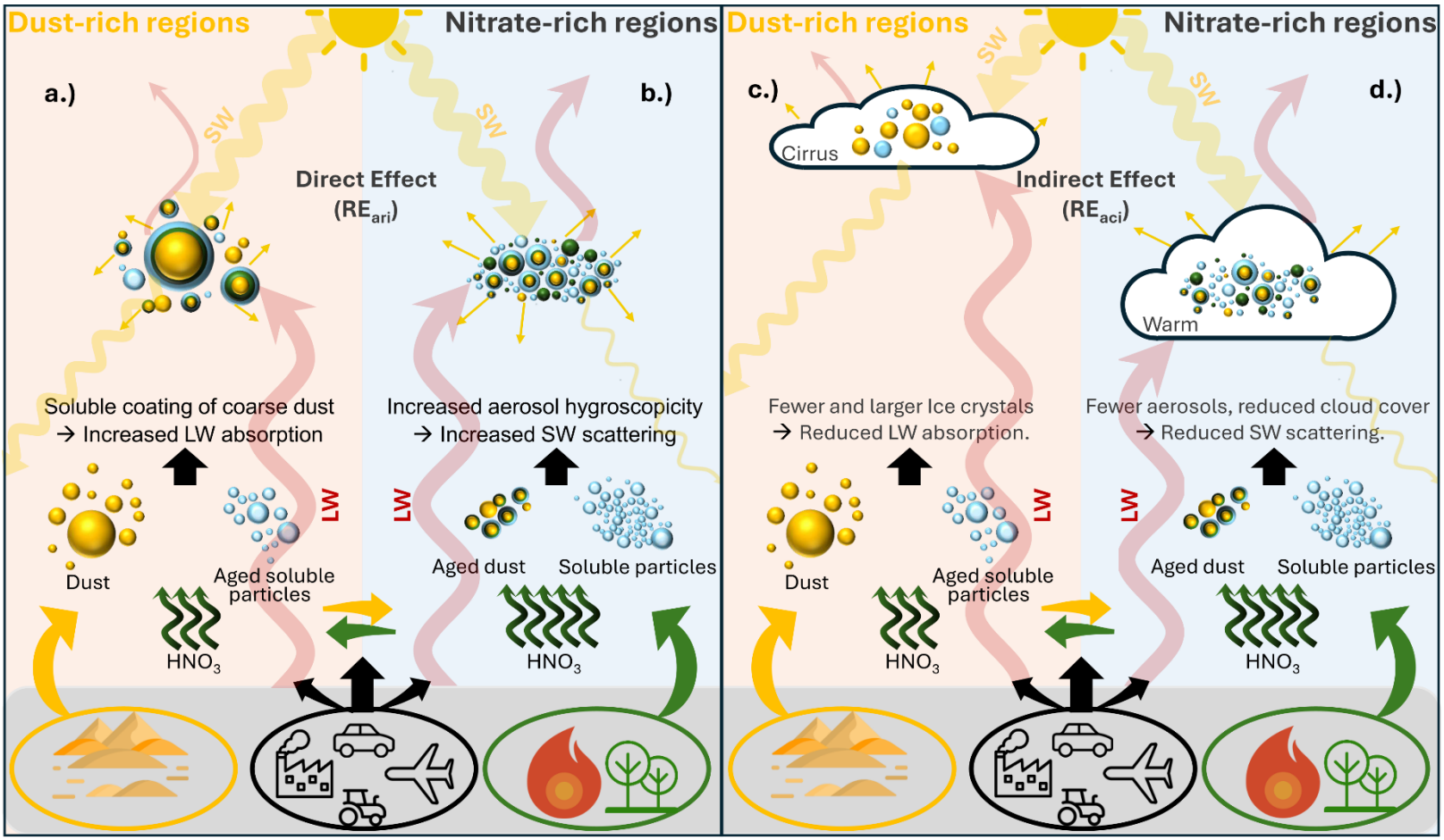

Figure 1 : Conceptual illustration of how dust-nitrate interactions affect the total NO_3^- (left) RE_{ari} and (right) RE_{aci}. a) In dust-rich environments, nitric acid transported from anthropogenic pollution and biomass burning regions interacts with mineral cations to form a soluble coating on the surface of dust particles. The dominant effect of these interactions is an enhanced LW absorption (warming RE_{ari}) by the coarse dust particles. **b.)** In nitrate-rich environments, the intrusion of dust particles and their subsequent interaction with freshly emitted nitric acid leads to an overall increase in aerosol hygroscopicity and thus a stronger SW reflection (cooling RE_{ari}). **c.)** In dust-rich environments, the number of ice crystals in cirrus clouds is reduced while their size is increased due to the interaction of dust particles with the transported HNO_3. This results in an optical thinning of the ice clouds, which leads to less trapping of outgoing LW radiation (cooling RE_{aci}). **d.)** In nitrate-rich environments, the increased wet radius of aged dust particles leads to enhanced coagulation with smaller particles, resulting in a decrease in the number of smaller aerosols and, in turn, a decrease in the number of activated particles in cloud droplets by smaller aerosols, which ultimately leads to a reduction in the backscattering of SW radiation by warm clouds (warming RE_{ari}).

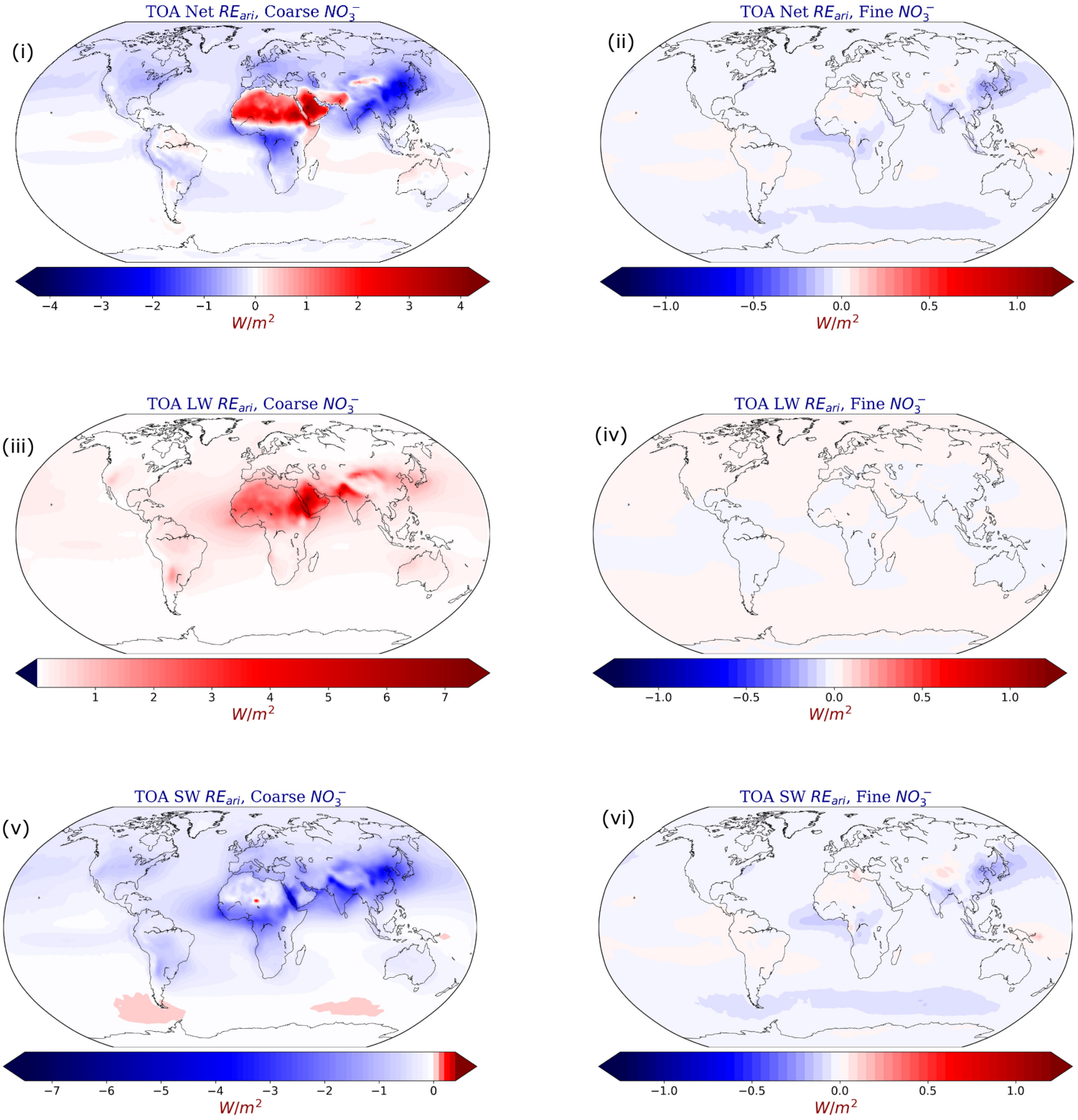

Figure 2: Global mean TOA net RE_{ari} for (i) coarse and (ii) fine NO3 aerosols; longwave RE_{ari} for (iii) coarse and (iv) fine NO3 aerosols; shortwave RE_{ari} for (v) coarse and (vi) fine NO3 aerosols, as calculated by EMAC from the base case simulation.

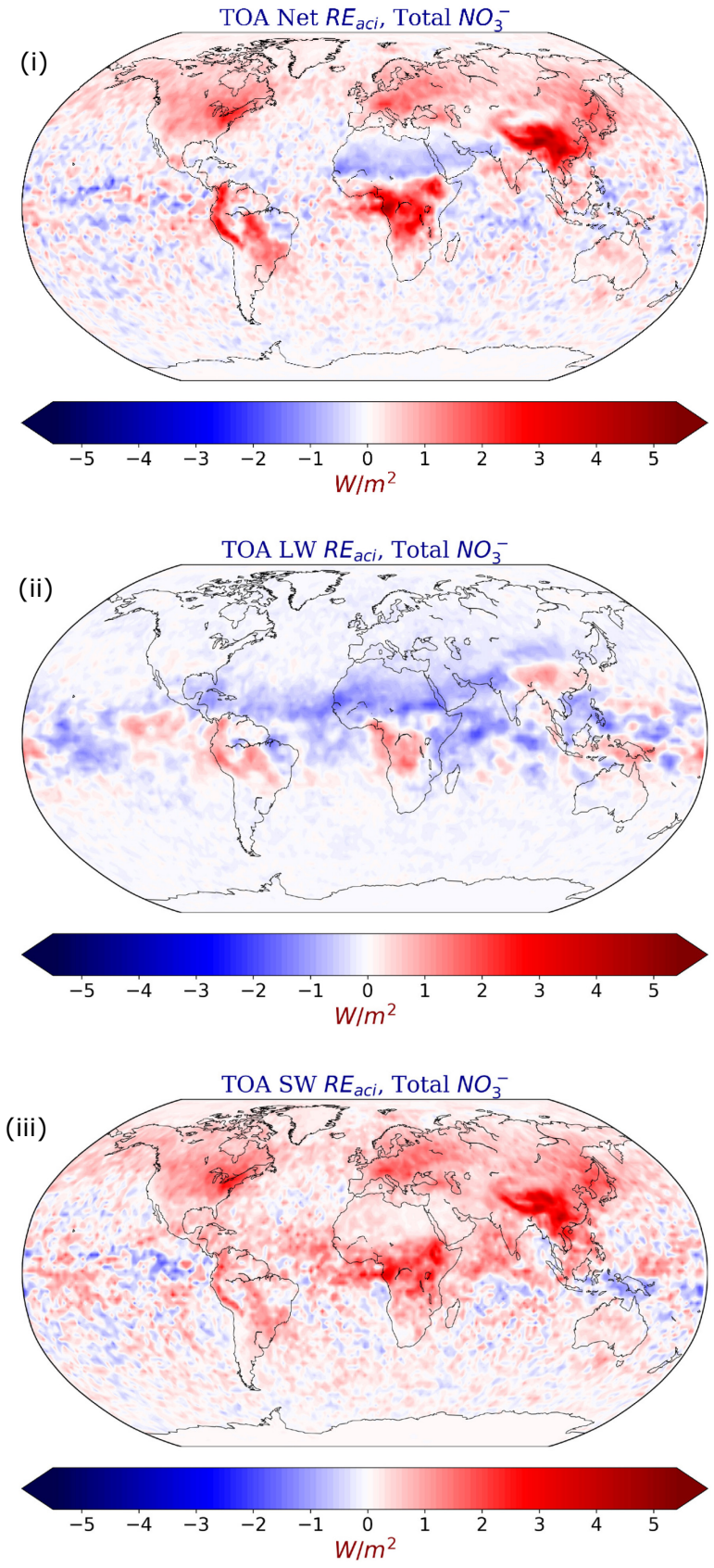

Figure 3: Global mean TOA RE_{aci} for total NO_3^- aerosols. Estimates for (i) net, (ii) longwave, and (iii) shortwave, as calculated by EMAC from the base case simulation.

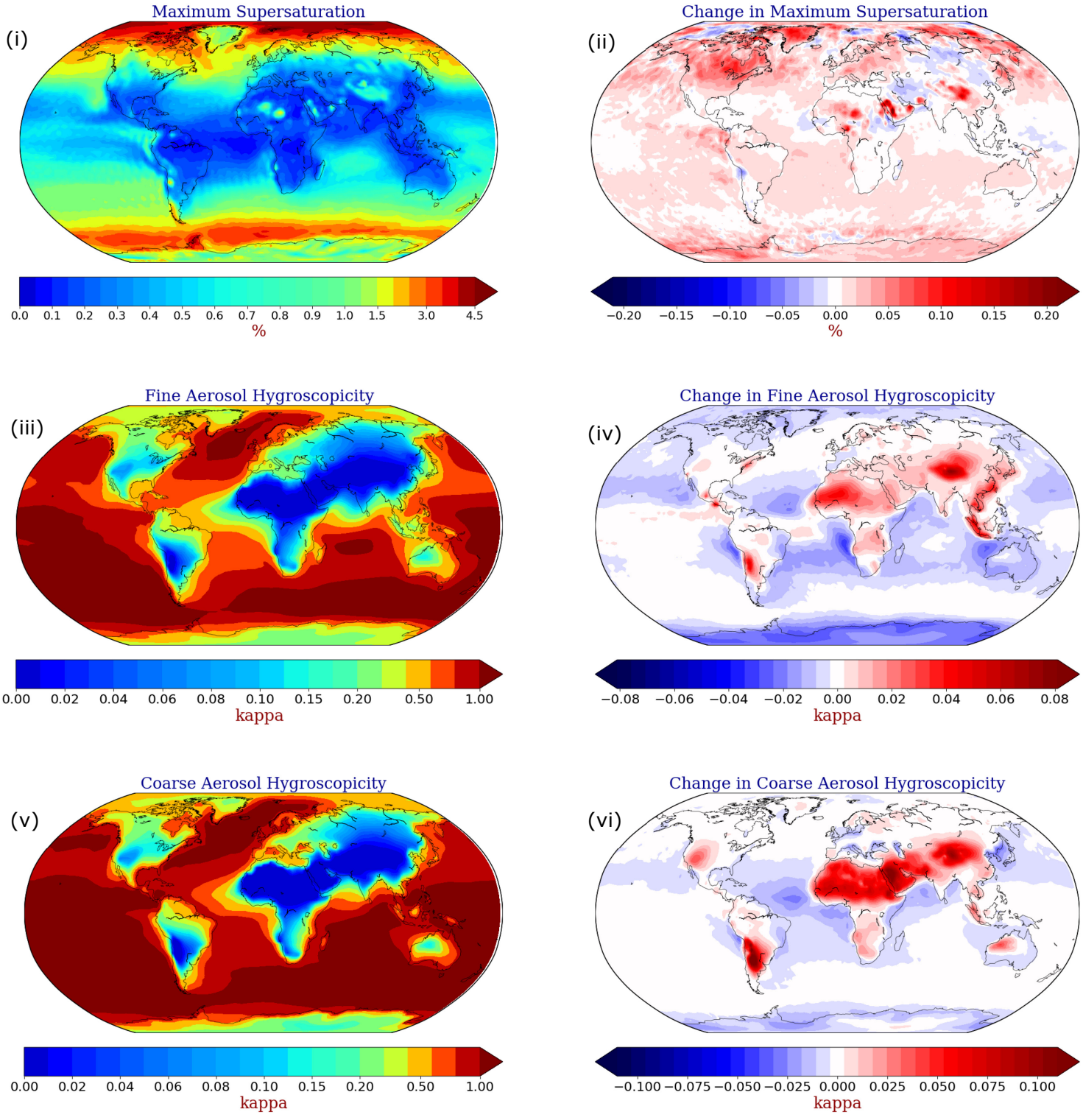
Maximum Supersaturation
(i)
0.0 0.1 0.2 0.3 0.4 0.5 0.6 0.7 0.8 0.9 1.0 1.5 3.0 4.5
%
Change in Maximum Supersaturation
(ii)
−0.20 −0.15 −0.10 −0.05 0.00 0.05 0.10 0.15 0.20
%
Fine Aerosol Hygroscopicity
(iii)
0.00 0.02 0.04 0.06 0.08 0.10 0.15 0.20 0.50 1.00
kappa
Change in Fine Aerosol Hygroscopicity
(iv)
−0.08 −0.06 −0.04 −0.02 0.00 0.02 0.04 0.06 0.08
kappa
Coarse Aerosol Hygroscopicity
(v)
0.00 0.02 0.04 0.06 0.08 0.10 0.15 0.20 0.50 1.00
kappa
Change in Coarse Aerosol Hygroscopicity
(vi)
−0.100 −0.075 −0.050 −0.025 0.000 0.025 0.050 0.075 0.100
kappa

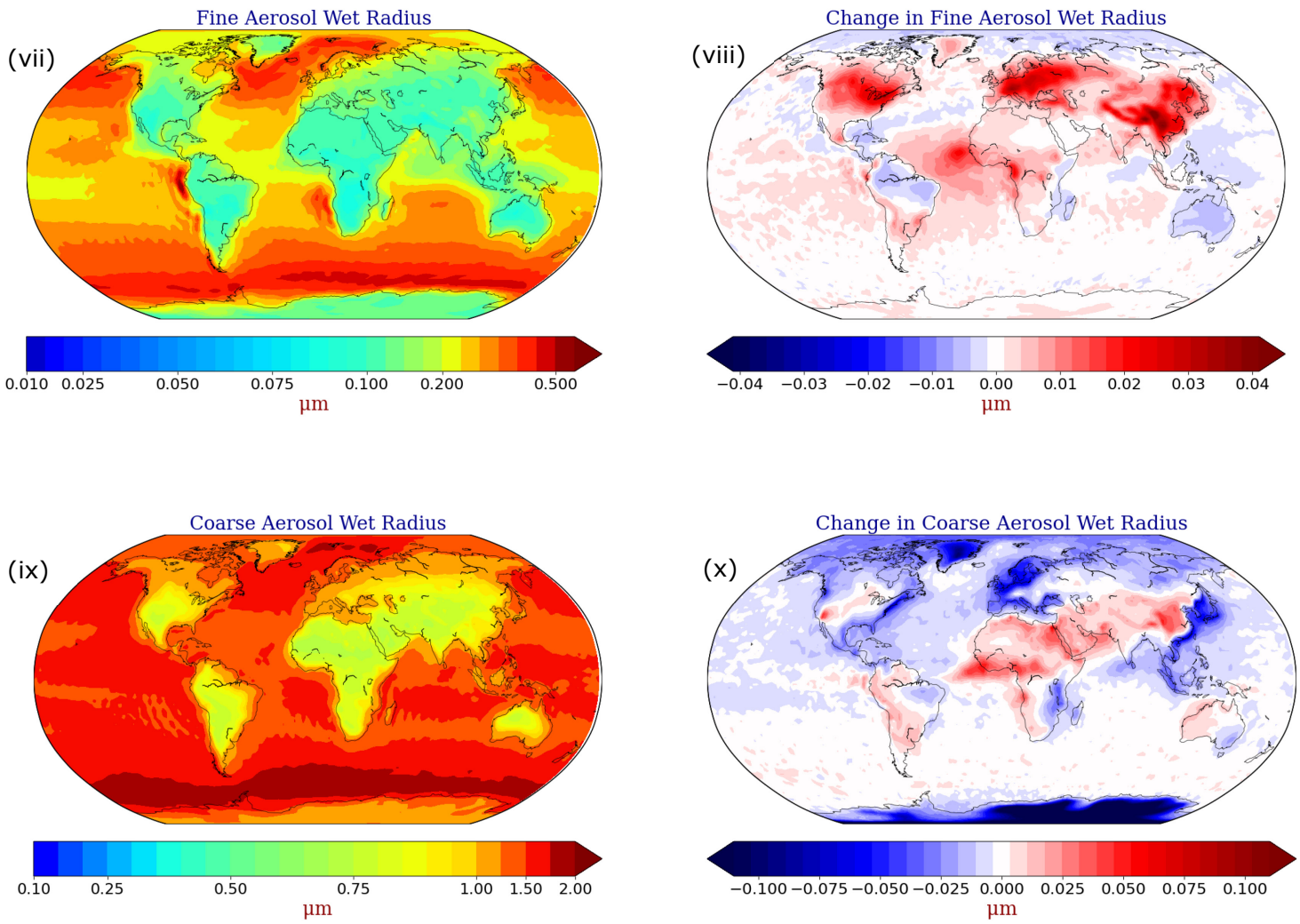

Figure 4: (i) Global mean maximum supersaturation, fine aerosol (iii) hygroscopicity and (v) wet radius, and coarse aerosol (vii) hygroscopicity and (ix) wet radius, as calculated by EMAC from the base case simulation. Absolute difference between base case and Nitrate Aerosol Free (NAF) sensitivity simulation in (ii) maximum supersaturation, fine aerosol (iv) hygroscopicity and (vi) wet radius, and coarse aerosol (viii) hygroscopicity and (x) wet radius. Red indicates higher values calculated by the base case simulation in the presence of NO_3^- aerosols.

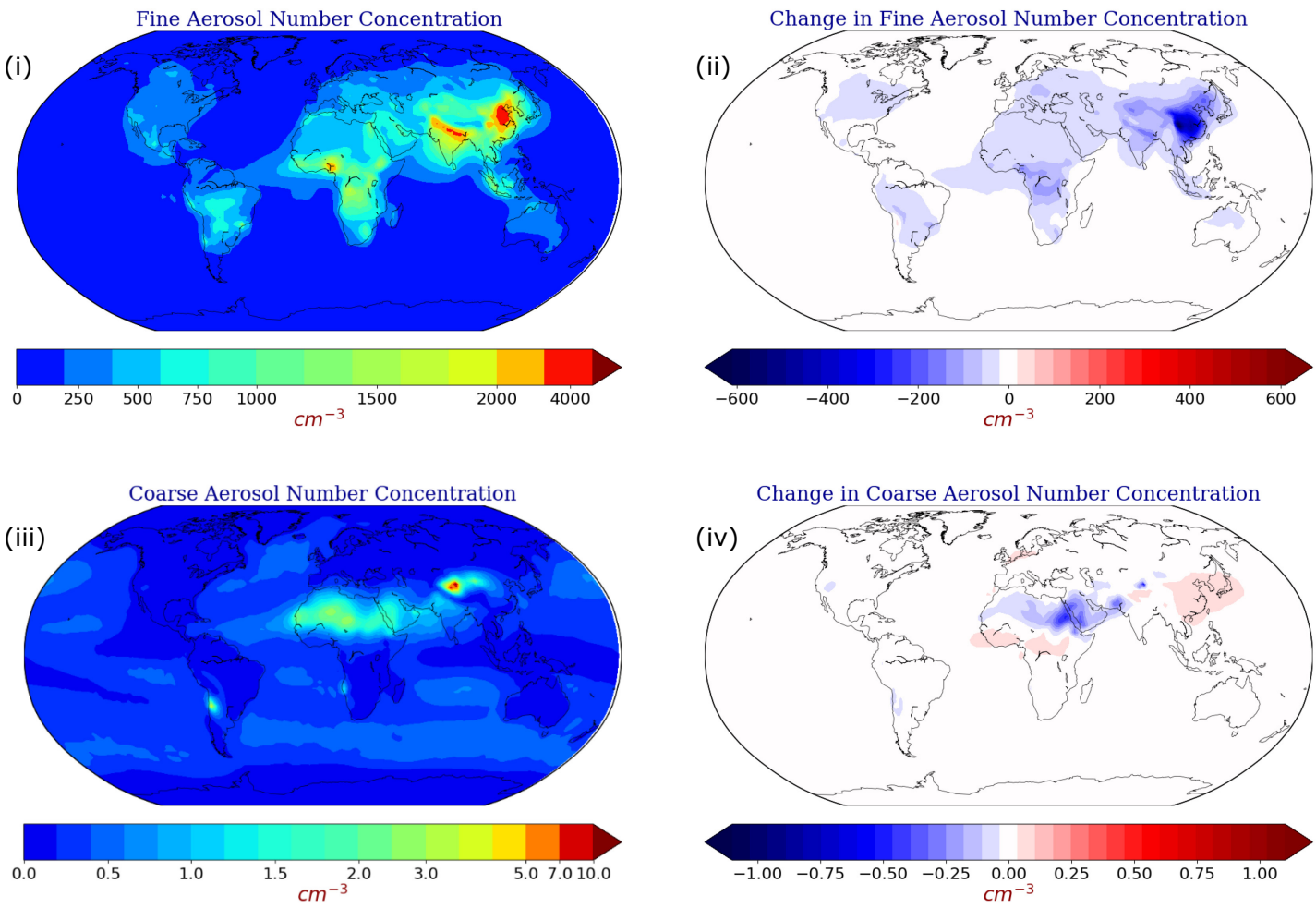

Figure 5: Global mean number concentration of (i) fine and (iii) coarse aerosols as calculated by EMAC from the base case simulation. Absolute difference between the base case and the Nitrate Aerosol Free (NAF) sensitivity simulation in the number concentration of (ii) fine and (iv) coarse aerosols. Blue indicates that number concentrations are lower in the presence of NO_3^- aerosols.

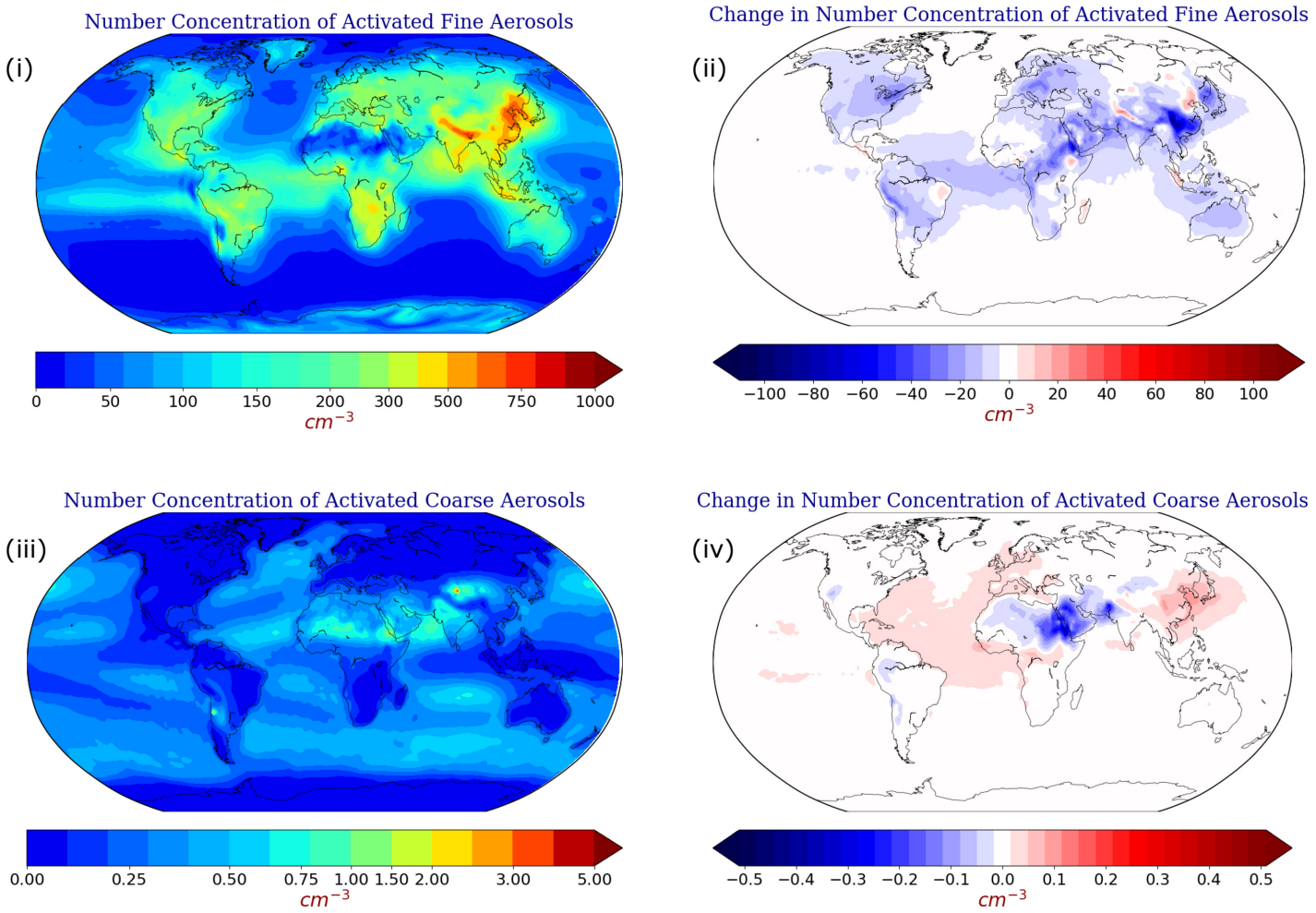

Figure 6: Global mean number concentration of activated (i) fine and (iii) coarse aerosols as calculated by EMAC from the base case simulation. Absolute difference between the base case and the Nitrate Aerosol Free (NAF) sensitivity simulation in the number concentration of activated (ii) fine and (iv) coarse aerosols. Blue indicates that number concentrations are lower in the presence of NO_3^- aerosols.